8-7-2020

Complex Tissue Regeneration in Mammals Is Associated with Reduced Inflammatory Cytokines and an Influx of T Cells

Thomas R. Gawriluk
University of Kentucky, tgawriluk@uky.edu

Jennifer Simkin
University of Kentucky, jennifer.simkin@uky.edu

Corin K. Hacker
University of Kentucky

John M. Kimani
University of Nairobi, Kenya

Stephen G. Kiama
University of Nairobi, Kenya

See next page for additional authors

Repository Citation

Authors

Thomas R. Gawriluk, Jennifer Simkin, Corin K. Hacker, John M. Kimani, Stephen G. Kiama, Vanessa O. Ezenwa, and Ashley W. Seifert

Complex Tissue Regeneration in Mammals Is Associated with Reduced Inflammatory Cytokines and an Influx of T Cells

Complex Tissue Regeneration in Mammals Is Associated With Reduced Inflammatory Cytokines and an Influx of T Cells

Thomas R. Gawriluk[1]*, Jennifer Simkin[1†], Corin K. Hacker[1], John M. Kimani[2], Stephen G. Kiama[2], Vanessa O. Ezenwa[3,4] and Ashley W. Seifert[1,2]*

[1] Department of Biology, University of Kentucky, Lexington, KY, United States, [2] Department of Veterinary Anatomy and Physiology, University of Nairobi, Nairobi, Kenya, [3] Odum School of Ecology, University of Georgia, Athens, GA, United States, [4] Department of Infectious Disease, College of Veterinary Medicine, University of Georgia, Athens, GA, United States

While mammals tend to repair injuries, other adult vertebrates like salamanders and fish regenerate damaged tissue. One prominent hypothesis offered to explain an inability to regenerate complex tissue in mammals is a bias during healing toward strong adaptive immunity and inflammatory responses. Here we directly test this hypothesis by characterizing part of the immune response during regeneration in spiny mice (*Acomys cahirinus* and *Acomys percivali*) vs. fibrotic repair in *Mus musculus*. By directly quantifying cytokines during tissue healing, we found that fibrotic repair was associated with a greater release of pro-inflammatory cytokines (i.e., IL-6, CCL2, and CXCL1) during acute inflammation in the wound microenvironment. However, reducing inflammation via COX-2 inhibition was not sufficient to reduce fibrosis or induce a regenerative response, suggesting that inflammatory strength does not control *how* an injury heals. Although regeneration was associated with lower concentrations of many inflammatory markers, we measured a comparatively larger influx of T cells into regenerating ear tissue and detected a local increase in the T cell associated cytokines IL-12 and IL-17 during the proliferative phase of regeneration. Taken together, our data demonstrate that a strong adaptive immune response is not antagonistic to regeneration and that other mechanisms likely explain the distribution of regenerative ability in vertebrates.

Keywords: spiny mice, regeneration, inflammation, cytokines, adaptive immunity, T cells, wild animal

INTRODUCTION

In response to damage, vertebrate tissue regeneration occurs as a chronological and overlapping series of processes that includes hemostasis, inflammation, re-epithelialization, activation of local progenitor cells, tissue morphogenesis, and replacement of the injured tissue. In contrast, most mammals heal injuries by fibrotic repair characterized by limited cellular proliferation and intense collagen deposition that results in scar tissue patching the injured wound (1). As with any trauma or infection that disrupts tissue architecture, regeneration and fibrotic repair are concomitant with a multiphasic immune response that promotes hemostasis, creates inflammation, protects against microbial infection, stimulates re-epithelialization, and stimulates a local fibrotic response (2). During most instances of regeneration (e.g., limb, fin, digit tip, etc.) there is an apparent resolution of inflammation that coincides with the accumulation of resident progenitor cells that

subsequently re-enter the cell cycle and self-organize to undergo morphogenesis (3, 4). This transition from an inflammatory environment to morphogenesis is synonymous with formation of a regenerative blastema (5). As such, the injured tissue must precisely coordinate dynamic interactions between cells and factors (i.e., cytokines, chemokines, growth factors etc.) within the injury microenvironment to resolve the inflammatory response and promote blastema formation.

Despite a rich literature describing the effects of immune cells and their products in non-regenerating wounds [reviewed in (6, 7)], our knowledge of the immune response during tissue regeneration remains relatively poor (8–10). Recent studies in fish, frogs, salamanders, and spiny mice support that immune cells and their products are required for blastema formation and successful regeneration. For example, when macrophages are removed during appendage amputation in adult fish or salamanders subsequent re-epithelialization, blastema formation and regeneration is prevented (11–13). Similar findings have been observed during neonatal mouse heart (14), adult mouse digit tip (15), and adult spiny mouse ear pinna regeneration (16), suggesting macrophages provide a necessary component to transition from wound healing to regeneration during vertebrate regeneration (5). The complete or timed depletion of regulatory T cells (T$_{REG}$) has also been tested, and similarly prevents zebrafish fin (17) and mouse skeletal muscle regeneration (18). Additionally, blocking reactive oxygen species production—a major inflammatory signal from macrophages and T cells—elicits a similar outcome in frog and zebrafish tail regeneration (19–21). Interestingly, even where regeneration does not occur through a blastema there is evidence for the upregulation of the immune response concurrent with regeneration, such as during spinal cord injury in neonatal opossum (22) or skin regeneration in spiny mouse (23). Perhaps not unexpectedly, similar experiments in non-regenerating systems cause incomplete wound closure and angiogenesis, suggesting that the same immune signals initiate fibrotic repair and regeneration (24–29). Moreover, when comparing the immune response to injury between fetal and adult mammals (30–32), pre- and post-metamorphic amphibians (33–35), closely-related regenerating and non-regenerating vertebrates (23), and regeneration-competent and scarring tissues in the same animal (36–38), all these studies support that reduced inflammation and a muted immune response are coincident with regeneration over fibrotic repair. Based on these results, the bias in the mammalian healing response toward strong adaptive immunity and inflammatory responses has emerged as one prominent hypothesis explaining the lack of regenerative capacity in this group. However, there are few robust tests of this hypothesis and an important series of studies support the idea that some inflammatory immune cells are passive participants during tissue regeneration. For example, removal of the spleen (39), or induction of leukopenia (40) during newt limb regeneration demonstrate that a severely reduced leukocyte response does not prevent blastema formation or regeneration.

These contrasting viewpoints raise several unanswered questions. (1) Are there specific factors produced by immune cells that polarize local cell phenotypes and specifically promote regeneration or fibrotic repair? (2) Does the inflammatory response impede blastema formation and subsequent regeneration in adult mammals? (3) Are the initial stages of fibrotic repair and regeneration driven by different immune responses, such that altering the immune response could stimulate regeneration in lieu of fibrotic repair? In this study, we directly test the prevailing hypothesis that inflammation compromises regeneration and provide much needed insight into the immune mechanisms that coincide with mammalian regeneration. We do this by following-up on the recent discovery that multiple species of spiny mice (e.g., *Acomys cahirinus, A. percivali, A. kempi*) regenerate skin and musculoskeletal tissue as fully immunocompetent adults (16, 41–43). Specifically, we characterize and compare the cytokine response to injury during fibrotic repair and regeneration to test if the immediate immune response to injury is different between these two healing outcomes. We compare the injury response using a 4 mm ear punch assay among three species (*A. cahirinus, A. percivali,* and *M. musculus*) and two source populations (wild-caught *A. percivali* and *M. musculus*, and laboratory-reared *A. cahirinus* and *M. musculus*) using a panel of sixteen cytokines (**Figures 1A,B**). Intriguingly, our results show that injury across all groups induces a common set of pro-inflammatory cytokines and leukocyte chemotactic factors supporting that some signals of acute inflammation are a shared feature of regeneration and fibrotic repair. We also find a faster, stronger, and prolonged adaptive immune response during regeneration, which suggests that a strong adaptive immune response is not antagonistic to regeneration.

MATERIALS AND METHODS

Animals

Mus musculus (Mm-UKY) and *Acomys cahirinus* (Ac) were maintained at our animal facility at the University of Kentucky, Lexington, KY, USA. Mm-UKY were sexually mature (10- to 12-week old), female, outbred Swiss Webster (ND4, Envigo, Indianapolis, IN). They were housed at a density of 2–4 individuals in static IVC cages with pine shavings and given autoclaved water and 18% protein mouse chow (Tekland Global 2918, Envigo). Ac were sexually mature (12- to 28-weeks old), males and females and were housed at a density of 10–15 individuals in large metal wire cages (24 inch × 12 inch × 14 inch, height × width × depth, Quality Cage Company, Portland, OR) with pelleted pine bedding (Southern States Cooperative, Inc., Richmond, VA) and given autoclaved water and a 3:1 mixture by volume of 14% protein mouse chow (Teklad Global 2014, Envigo) and black-oil sunflower seeds (Pennington Seed Inc., Madison, GA) (44). The temperature was maintained at 23°C with 50% humidity and the animals were exposed to natural light through large windows (∼12:12 h L:D light cycle during the experiment). All Mm-UKY and Ac samples were collected between 9/20/2015 and 10/28/2015.

Wild *M. musculus* (Mm-Wild) were live-trapped at the C. Oran Little Research Center in Versailles, KY (38°4'N, 84°44'W) and maintained in an alternate animal facility at the University of Kentucky. Mm-Wild were housed at a density of 10–12
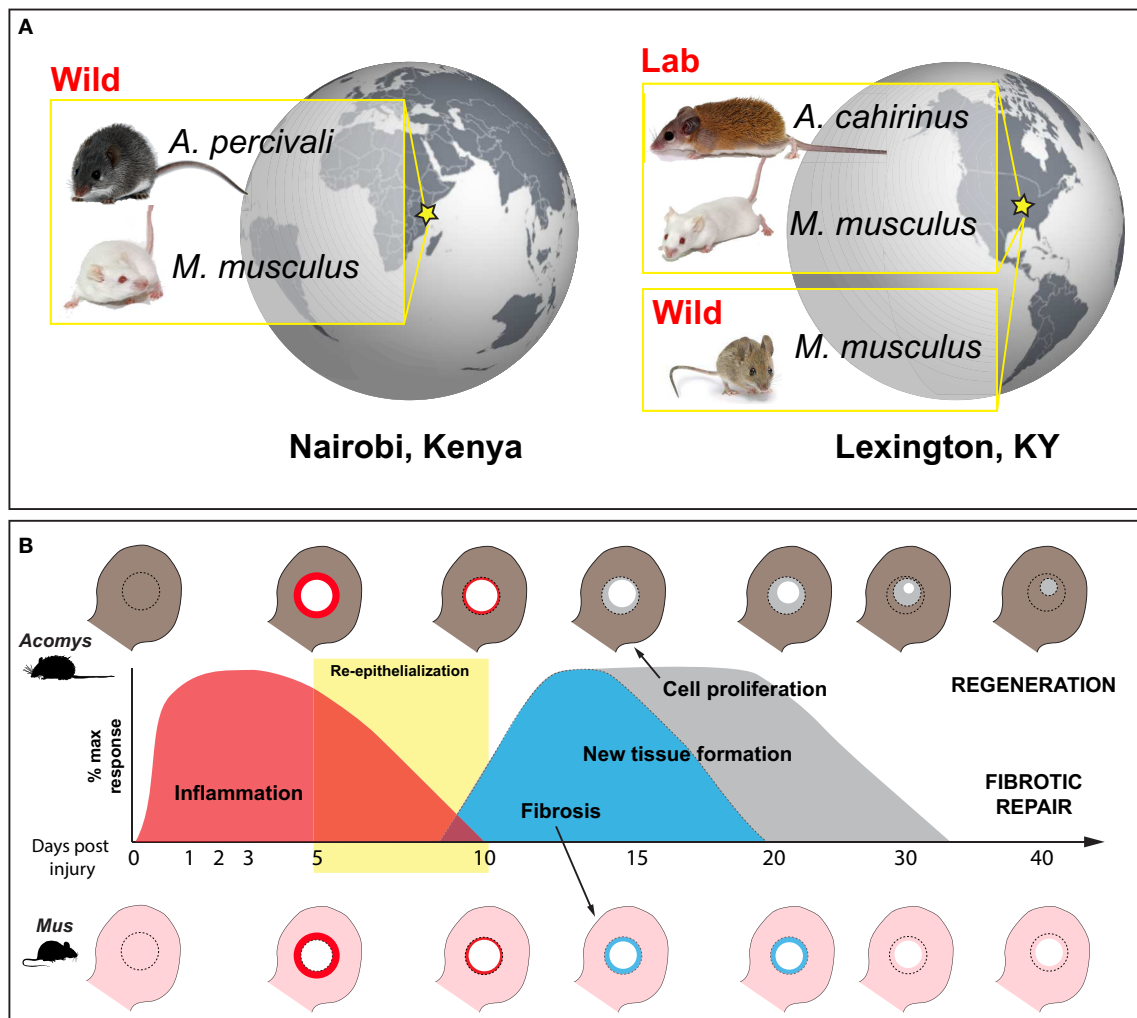
FIGURE 1 | Wild-caught and laboratory-reared animals employed to characterize the immune response to injury during regeneration and fibrotic repair using a comparative ear punch assay. **(A)** Immune-primed *A. percivali* (wild-caught) and *M. musculus* (privately bred) were acquired in Kenya and housed in an open-air facility in Nairobi. *A. cahirinus* and *M. musculus* used at the University of Kentucky were captive bred from lab colonies in a clean facility and considered to have naïve immune systems. We also trapped *M. musculus* in Kentucky. **(B)** Schematic depicting excision of a 4 mm circular hole in the ear pinna (D0) and subsequent regeneration and fibrotic repair in *Acomys* and *Mus,* respectively. Local inflammation follows tissue excision and persists until ~D10 (red) (16, 42). Keratinocyte activation leads to re-epithelialization between D5 and D10 (yellow box) (41, 43). New tissue formation follows re-epithelialization and is characterized by a strong upregulation of extracellular matrix proteins. Matrix production is biased toward collagen production and fibrosis in *Mus*, leading to scar formation and an open hole (light blue). In *Acomys*, robust cell proliferation is maintained until the entire hole is filled with new tissue that undergoes morphogenesis to replace all of the original tissue components (e.g., epidermis, dermis, hair follicles, sebaceous glands, cartilage, etc.) (gray).

individuals in large metal wire cages with pelleted pine bedding and given autoclaved water and 18% protein mouse chow. The animals acclimated to captivity for at least 21 days before any experiments were started. The air within the facility was filtered, temperature was maintained at 23°C with 50% humidity and the animals were exposed to a 12:12 h L:D cycle by fluorescent lights. All Mm-Wild samples were collected between 4/1/2017 and 6/21/2017 and 12/12/2017 and 3/6/2018.

The Kenyan *M. musculus* (Mm-Kenya) were sexually mature (10- to 12-week old), female, outbred Swiss Webster mice obtained from a local breeder in Nairobi, Kenya and maintained in an animal facility at the University of Nairobi, Kenya.

Sexually mature *Acomys percivali* (Ap) were live-captured at Mpala Research Centre in Laikipia, Kenya (0°17'N, 37°52'E), and transported to the University of Nairobi for study. Each species was separated by sex and housed at a density of 10–15 animals in large metal wire cages, given tap water, fed mouse pencils (Argrocide Inc., Nairobi, Kenya) 1 × per day and exposed to natural light through windows (equivalent 12 h:12 h L:D cycle). The animals acclimated to captivity for at least 21 days before any experiments were started. Additionally, the facility was open to the natural environment (i.e., the mice were exposed to Nairobi air), the average daytime temperature was 22.7°C and cooler nighttime temperatures were supplemented with ceramic

heaters. Mm-Kenya samples were collected between 6/04/2015 and 7/04/2015 and Ap samples were collected between 5/04/2015 and 7/04/2015, and between 5/02/2016 and 6/04/2016.

All animal trapping and procedures were approved by the University of Kentucky Institutional Animal Care and Use Committee (IACUC) under protocol 2013-1119, Kenyan Wildlife Service (KWS), and the University of Nairobi Faculty of Veterinary Medicine Animal Care and Use Committee (FVM ACUC). Research in Kenya was approved by the Kenyan National Council for Science and Technology (NACOSTI). All wild species trapped were species of least concern. A summary of animals used for each experiment can be found in **Table S1**.

Sample Collection and Preparation

We used a 4 mm biopsy punch to create a hole through the ear pinna, as previously described (41). Healing ear tissue was collected on (D)ay 0, 1, 2, 3, 5, 10, 15, and 20. To minimize possible circadian effects, animals were injured between 10:00 and 12:00, and samples were collected between 11:00 and 15:00. Animals were deeply anesthetized with 5% (v/v) isoflurane and a maximal amount of blood was collected by cardiac puncture using a 25-gauge needle. An 8 mm biopsy punch was used to harvest healing ear tissue.

To isolate serum, blood was collected into a serum separator tube (#454243, Greiner bio-one, Kremsmünster, Austria) and allowed to clot for at least 45 min, followed by centrifuging at 3,000 × g for 10 min. Serum was aliquoted and stored at −80°C or on dry ice until analysis. The tissue was used for two downstream assays, histology and cytokine quantification. For histology, one of the 8 mm biopsies was placed into 10% (v/v) neutral buffered formalin (American MasterTech, McKinney, TX) overnight, dehydrated, embedded in paraffin and cut to 5 µM thickness on a rotary microtome. For cytokine quantification, a ring of tissue closest to the injury ~1 mm wide was snap frozen in liquid nitrogen or a slurry of dry ice and ethanol, and then stored at −80°C or on dry ice. Next, the tissue was homogenized in RIPA buffer supplemented with protease and phosphatase inhibitors (#24948, Santa Cruz Biotechnology, Inc. Dallas, TX; #78427, Thermo Scientific) using ceramic beads (Matrix D, MP Biomedicals, LLC, Solon, OH) and a bead mill for 5 min (Next Advance, Inc., Troy, NY), centrifuged at 10,000 × g for 15 min to pellet insoluble protein, and the soluble protein was separated into a new tube. The total soluble protein was quantified by bicinchoninic acid assay (#23225, Thermo Scientific) with a standard curve created from the same stock of bovine serum albumin, and then the protein lysate was stored at −80°C or on dry ice until analysis.

Cytokine Assay

To assess the immune response to injury in multiple species, we evaluated methods that: (1) used minimal sample, (2) measured local (tissue lysate) and systemic (serum) samples, (3) measured several cytokines at once, (4) differentiated the magnitude and type of immune response during an ear punch assay, and (5) exhibited cross-reactivity among the study species. We used a custom-designed, multiplexed, sandwich ELISA array (Quansys Biosciences, Logan UT). This platform meets the above

requirements and the experiments can be performed in multiple locations (i.e., Kentucky and Kenya) because the imager and reagents can be easily transported. Importantly, the imager does not require specialized calibration after being moved, and the reagents do not need to remain frozen. The custom assay was designed to measure 16 antigens including IL-1α, IL-1β, IL-2, IL-4, IL-5, IL-6, IL-10, IL-12p70, IL-17, CCL2, CCL3, CCL5, CSF2, IFNγ, TNFα, and CXCL1. Quansys Biosciences uses commercially available polyclonal and monoclonal antibodies to design their sandwich ELISAs for each target. We selected from a list of 22 cytokines for inclusion on the plate assay. In selecting specific cytokines, we targeted cytokines (1) with known pro- and anti-inflammatory properties, (2) that were associated with chemotaxis of immune cells and (3) that were specifically associated with macrophage and T cell phenotypes.

Initial testing identified that antigens from serum could be quantified by diluting serum in the supplied mouse specific diluent 1:1 and from tissue lysate using 5, 40, and 80 µg total protein in RIPA buffer for *M. musculus*, *A. cahirinus*, and *A. percivali*, respectively. The samples were run in duplicate using a protocol modified from the manufacturer's instructions, as follows: All serum samples were diluted 1:1 (serum: diluent) and all tissue samples were diluted 1:1 (RIPA + lysate: mouse sample diluent) to a volume of 50 µL per well. The diluted samples were then loaded onto a new assay plate with an appropriate standard curve (1:3 to 1:59049) and four blanks. Samples were incubated at 4°C for 8 h on a plate shaker set to 500 rpm to capture antigen in each well. After washing the plate 4 times with wash buffer, the primary antibody cocktail was loaded and the plate was incubated at 4°C for 8 h on a plate shaker set to 500 rpm to allow binding of the biotinylated detection antibodies to the captured antigens. After washing the plate 4 times, streptavidin-HRP conjugated secondary antibody cocktail was loaded and the plate was incubated at room temperature for 30 min on a plate shaker set to 500 rpm. The plate was washed 8 times, chemiluminescent reagent was added, and the plate was immediately imaged with a chemiluminescent plate imager set to the manufacturer recommended image capture settings (Q-view imager, Quansys Biosciences).

We verified that cytokine concentrations derived from the Quansys multiplex array were comparable between *Mus* and *Acomys* by testing for parallelism of the mouse standards with *Acomys* serum and tissue lysate. We also evaluated the peptide-level similarity between *Mus* and *Acomys* for each gene represented on the array. Parallelism was examined using standard protocols (45, 46). Briefly, samples from species and source were randomly pooled to provide a representative cytokine concentration and were run in triplicate at serial dilutions (1:2, 1:6, 1:18, 1:54, and 1:162). To determine parallelism, linear regressions were calculated for samples that had at least 3 dilutions above the lower limit of detection and we compared the slopes to the standard curve. For peptide comparisons, the *A. cahirinus* genomic and/or transcribed sequences corresponding to the 16 cytokines of interest were identified by using TBLASTX with inputted *M. musculus* peptide sequence into previously published spiny mouse transcriptomes (41, 47) and an unpublished draft genome. The mRNA sequence

was then translated and aligned to peptide sequences for *M. musculus*, *Rattus norvegicus* and *Homo sapiens* using MAFFT (48, 49). Total similarity and identity was calculated using the Sequence Identity and Similarity (SIAS) tool (http://imed.med. ucm.es/Tools/sias.html).

Individual cytokine concentrations were obtained using image analysis software (Q-view v3.09, Quansys Biosciences). First, the standard curve pixel intensity values were observed and pixel intensity values <60,000 were masked to remove saturated data points. Sample concentrations were calculated from standard curves created by a five-parameter logistic regression (5PL) with $\sqrt{y}$ weighting. The average value from each duplicate was then used for subsequent analyses. If the average value was above the lower limit of detection and the pixel intensity co-efficient of variation between duplicates was <15%, the sample was re-assayed on another plate and a new average calculated. Initially, we re-assayed tissue samples below the limit of detection with a greater amount of total protein, but in most cases, additional protein did not equate to quantifiable antigen, suggesting that there was a minimal amount of antigen in those samples. Thus, to maximize use of the plates, we opted to quantify a greater total number of samples and assayed each sample at one dilution. Antigens below the lower limit of detection were recorded as "not present," and to calculate ratios they were assigned the largest value of the lower limit of detection for that antigen across all plates assayed (50).

COX-2 Inhibition

Mm-UKY were subjected to a routine ear punch assay and randomly split into two groups: (A) 100 mg/kg celecoxib, a potent and specific COX-2 inhibitor or (B) vehicle. A Celecoxib capsule was opened and mixed into 0.5% (w/v) methyl cellulose to the appropriate concentration and a 200 µL dose was administered (100 mg active drug/kg body weight) by oral gavage using a 20 × 30 mm gavage needle tipped with a sugar solution each morning beginning 1 day before injury through 20 days after injury. Ear holes were measured and ear hole area was calculated for every 5 days post injury, as previously described (41). On D10 and 64 entire ears were harvested from a different set of animals and used for histology and stained with Mason's Trichrome or Picrosirius red, as previously described (41). Re-epithelialization was confirmed by the presence of a connected and complete epidermis distal to the amputation plane by examining two tissue sections from the proximal and distal wound sites for each animal at D10. Fibrosis was determined by quantifying the area of collagen deposition in the dermis distal from the amputation plane from two sections from the proximal and distal wound sites using circular polarized light microscopy and the thresholding function in Image J after removing the epidermis, epidermal appendages and tissue artifacts.

Flow Cytometry

To quantify the number of CD3+ cells present in healing ear tissue, tissue was harvested from a separate group of Mm-UKY and Ac females at D0, 1, 3, 7, and 15 using an 8 mm biopsy punch. Harvested tissue from both ears was combined and a single-cell suspension was created using a combination of enzymatic and mechanical digestion, as previously described (16). Total cells were counted by hemacytometer and incubated with PE-conjugated-anti-CD3 (Clone 17A2, BioLegend, San Diego, CA) at a concentration of 1 µg/10^6 cells for 1 hour at room temperature, washed and suspended in cell staining buffer (Cat#420201, BioLegend). Flow cytometry was carried out at the University of Kentucky Flow Cytometry Core using the iCyt Synergy sorter system (Sony Biotechnology Inc., San Jose, CA). Laser calibration and compensation was performed for each experiment using unstained and single fluorescent control samples. Analysis was done using FlowJo (Version 10, FlowJo, LLC, Ashland, OR) to identify CD3-positive lymphocytes by PE fluorescence and forward- and side-scatter. The same gating strategies between species were used ($n = 4$ or 5 animals per timepoint).

Immunohistochemistry

To identify the locations of STAT3-responsive cells and CD3+ cells, tissue sections were de-paraffinized, rehydrated, and prepared for examination by light- or fluorescence-microscopy, respectively. For light-microscopy, resident peroxidase was quenched by H_2O_2, antigens were exposed by heat-mediated retrieval with sodium citrate buffer, pH = 6.0, blocked with 2.5% horse serum (Vector Laboratories, S-2012), incubated with primary antibody (rabbit anti-pSTAT3, Cell Signaling Technology Cat#9145, 1:200) overnight at 4°C, incubated with a horseradish peroxidase conjugated secondary antibody (goat anti-rabbit, Santa Cruz Biotechnology, Cat#sc-2030, 1:1000) for 1 h at room temp, treated with 3,3'-Diaminobenzidine (SK-4100, Vector Laboratories, Burlingame, CA) until a visible brown precipitate was observed, counter-stained with hematoxylin, dehydrated and cover-slipped. For fluorescence-microscopy, antigens were exposed by heat mediated retrieval with sodium citrate buffer, pH = 6.0, resident avidin and biotin was blocked (Vector Laboratories, SP-2001). Sections were then blocked with 2.5% horse serum, incubated with primary antibody (rabbit anti-CD3, DAKO, Cat#A0452, 1:500) overnight at 4°C, incubated with a biotin conjugated, secondary antibody (goat anti-rabbit, Vector Laboratories, Cat#PK-6101, 1:400) for 1 h at room temp, incubated with streptavidin conjugated AlexaFlour-594 (Molecular Probes, Cat#S11227, 1:5,000), counter-stained with 4',6-Diamidino-2-Phenylindole, Dihydrochloride (Molecular Probes, Cat#D1306, 1:10,000) and cover-slipped. Images were acquired using a compound epi-fluorescence microscope (IX-51, Olympus Corporation, Tokyo, Japan) equipped with a CCD camera (DP-74, Olympus Corporation) and software (cellSens v1.12, Olympus Corporation).

Immunoblot

To quantify the STAT3 response to injury, 30 or 40 µg of total protein from tissue lystate was denatured and separated using gel electrophoresis on a 4–20% polyacrylamide gel and transferred to a PVDF membrane (IB401002, Life Technologies). In order to prevent the need for membrane stripping and to preserve sample, the membranes were cut along the 55 kDa ladder marker and blocked with either 5% BSA for pSTAT3 or 5% dry skim milk for ACTB in TBST for 1 h at room temperature. Membranes

were then incubated with primary antibody (rabbit anti-pSTAT3, Cell Signaling, Cat#9145, 1:2000; rabbit anti-ACTB, Cell Signaling, Cat#4967, 1:5000), washed with TBST, incubated with a horse radish peroxidase conjugated, secondary antibody (goat anti-rabbit, Santa Cruz Biotechnologies, Cat#sc-2030, 1:10,000), and visualized by chemiluminescence (Cat#RPN2235, GE Healthcare) using a digital CCD camera (UVP LLC, Upland, CA). Total pixel intensity was quantified using regions of interest and normalized to background and uninjured tissue using ImageJ2 (51).

Statistical Analysis

To compare the cytokine concentrations in the serum at baseline, we used a one-way ANOVA and Tukey-Kramer HSD *post-hoc* tests to test for group differences. To compare the dynamics of cytokine concentration over time in serum and tissue, a ratio of the injured concentration mean to the uninjured concentration mean was calculated for each cytokine by group (Mm-UKY, Mm-Kenya, Mm-Wild, Ac and Ap) and time point (D1-D20). To normalize cytokine fold-change distributions, data were log transformed and tested for normality using a Shapiro-Wilk test and *P*-value > 0.05. A two-way ANOVA was then used to test for effects of time and group on tissue and serum separately. Pairwise comparisons were tested using the Tukey-Kramer HSD method. In the event that several undetected values existed at an individual timepoint and log transformed data still did not meet normality, we used non-parametric Wilcoxon rank sum tests with Steel Dwass *post-hoc* tests for pairwise comparisons. Datasets for which non-parametric analyses were performed are indicated in figure legends.

To compare the immunoblot data, pixel intensity was calculated for the bands of interest using an identical sized region of interest with ImageJ (51). The pixel intensity of pSTAT3 was normalized to ACTB and a two-way ANOVA with time and species was used to compare values and pairwise comparisons were made using the Tukey-Kramer HSD method. To compare the flow cytometry results, we used a two-way ANOVA with time and species on log-transformed data and pairwise comparisons were made using the Tukey-Kramer HSD method. To compare the ear-hole closure rate between control and celecoxib-treated animals we used a repeated-measures ANOVA and cubic regression, as previously published (41). To compare the ear-hole area and area of tissue positive for Picrosirius, we used a Student's *t*-test. All statistical tests were done using JMP Pro 14 (SAS Institute Inc., Cary, NC) or Prism 5.0 (GraphPad Software, Inc., San Diego, CA). A *P*-value < 0.05 was used to determine significance for each test. All graphs were created in Prism 5.0 and placed into figures using Illustrator CS5 (Adobe Systems, Inc. San Jose, CA).

RESULTS

Cross-Species Validation of Cytokine Detection in Rodent Serum and Tissue

To begin characterizing the mammalian immune response during epimorphic regeneration, we analyzed 16 cytokines (Interleukin 1-alpha (IL-1α), IL-1β, IL-2, IL-4, IL-5, IL-6, IL-10, IL-12p70, IL-17, chemokine (C-C motif) ligand 2 (CCL2) (a.k.a. monocyte chemoattractant protein 1 or MCP-1), CCL3 (a.k.a. macrophage inflammatory protein 1α or MIP-1α), CCL5 (a.k.a. regulated on activation, normal T cell expressed and secreted or RANTES), colony-stimulating factor 2 (CSF2) (a.k.a. granulocyte-macrophage colony-stimulatory factor or GM-CSF), tumor necrosis factor-alpha (TNFα), interferon-gamma (IFNγ) and chemokine (C-X-C motif) ligand 1 (CXCL1) (a.k.a. KC)) using a custom-designed sandwich ELISA array. We used this assay to compare five groups: three at the University of Kentucky, (1) laboratory-reared, outbred *Mus musculus* (Mm-UKY), (2) wild-caught *M. musculus* (Mm-Wild), (3) laboratory-reared *Acomys cahirinus* (Ac), and two at the University of Nairobi, (4) outbred *M. musculus* reared by a local breeder (Mm-Kenya) and (5) wild-caught *A. percivali* (Ap) (**Figure 1A**). Our experimental design allowed us to compare cytokine responses between regenerating and non-regenerating species (Ac and Ap compared to Mm-UKY, Mm-Kenya and Mm-Wild), and between immune-challenged and laboratory-reared animals (Mm-Kenya, Mm-Wild, and Ap compared to Mm-UKY and Ac) (**Figure 1B**).

Parallelism analysis showed comparable slopes between *Mus* and *Acomys* serum and tissue samples with the mouse standard curve for a majority of cytokines (**Table 1** and **Figure S1**). Given non-parallel slopes, we did not validate using this assay to compare IL-10 or CCL5 between species (**Figure S1**). Several cytokines not present in *Acomys* serum were quantified in tissue lysate (Ac: IL-1β, IL-4, IL-6, IL-17, CSF2, CCL2; Ap: IL-17, CSF2, CXCL1) supporting that the serum concentration was below the limit of detection and that the antibody binding epitopes were conserved between species. Therefore, if the cytokine was detected in one tissue source or one *Acomys* species, we concluded it could be detected in the other source or species. This provided us with a way to determine if a cytokine was present or absent. A comparison of full-length predicted amino acid sequences between *A. cahirinus* and *M. musculus* indicated conservation—minimum of 56.8% (IFNγ) to a maximum of 95.8% (TNFα) (**Table 2** and **Data File S2A–Q**). Given that CXCL1 was the only cytokine not detected in the Ac samples, this supports that it was likely not present vs. a failure to detect it. Together, these results supported that the ELISA could be used to directly compare changes in the validated cytokines between species.

Fibrotic Repair Is Associated With Elevated Amounts of Circulating IL-5, IL-6, and CCL3

Using our cytokine assay, we first compared circulating serum cytokine concentrations from uninjured animals among groups (species and source population) to establish a systemic baseline for each group (**Figure 2**). A total of 13 cytokines were compared as CSF2 was not present in the serum of any species. While many baseline concentrations were similar between groups, immune-challenged animals (i.e., wild) exhibited higher IL-4, IL-6, CCL2, and TNFα compared to laboratory-reared animals (**Figure 2**). Interestingly, the Mm-Kenya animals were a

TABLE 1 | Comparison of cytokine slopes from parallelism test of cytokine assay.

Antigen	Standard	Sample	Mus musculus (Mm)	Acomys cahirinus (Ac)	Acomys percivali (Ap)	Comparison
IL-1α	−0.89 ± 0.03	Serum:	−1.05 ± 0.03*	−0.82 ± 0.14*	−1.37 ± 0.10*	Mm, Ac, Ap
		Tissue:	Too few points^	−1.03 ± 0.04*	−0.97 ± 0.18*	Mm, Ac, Ap
IL-1β	−0.93 ± 0.10	Serum:	Too few points&	Not detected	−1.63 ± 0.21*	Mm, Ap
		Tissue:	−0.94 ± 0.02*	−0.86 ± 0.03*	−0.65 ± 0.07*	Mm, Ac, Ap
IL-2	−1.34 ± 0.05	Serum:	Too few points&	Not detected	−0.87 ± 0.00*	Mm, Ap
		Tissue:	−1.21 ± 0.10*	−0.59 ± 0.22*	−0.57 ± 0.20*	Mm, Ac, Ap
IL-4	−0.89 ± 0.06	Serum:	−0.88 ± 0.18*	Too few points&	−2.16 ± 0.32*	Mm, Ap
		Tissue:	−0.69 ± 0.09*	−0.68 ± 0.39*	−0.75 ± 0.12*	Mm, Ac, Ap
IL-5	−1.13 ± 0.01	Serum:	−1.63 ± 0.20*	−1.53 ± 0.96*	−2.52 ± 0.28*	Mm, Ac, Ap
		Tissue:	−0.73 ± 0.05*	Too few points &	−0.87 ± 0.03*	Mm, Ap
IL-6	−1.07 ± 0.02	Serum:	−0.74 ± 0.12*	Too few points&	−1.81 ± 0.11*	Mm, Ap
		Tissue:	−0.80 ± 0.14*	−0.47 ± 0.06*	−0.63 ± 0.11*	Mm, Ac, Ap
IL-10	−1.56 ± 0.03	Serum:	Not detected	Not detected	Not detected	None
		Tissue:	Not detected	0.52 ± 0.25	0.24 ± 0.52	None
IL-12	−1.10 ± 0.02	Serum:	−0.68 ± 0.16*	−1.55 ± 0.49*	−1.26 ± 0.18*	Mm, Ac, Ap
		Tissue:	−0.73 ± 0.17*	−0.68 ± 0.16*	−0.63 ± 0.15*	Mm, Ac, Ap
IL-17	−1.03 ± 0.02	Serum:	−0.72 ± 0.25*	−0.16 ± 0.23	−0.49 ± 0.16	Mm
		Tissue:	−1.28 ± 0.04*	−0.85 ± 0.34*	−0.81 ± 0.03*	Mm, Ac, Ap
CSF2	−1.45 ± 0.05	Serum:	Not detected	Not detected	Too few points&	None
		Tissue:	−0.71 ± 0.11*	−0.68 ± 0.25*	−0.70 ± 0.10*	Mm, Ac, Ap
CCL2	−1.17 ± 0.00	Serum:	−1.23 ± 0.14*	Too few points&	−1.56 ± 0.13*	Mm, Ap
		Tissue:	−0.97 ± 0.02*	−1.23 ± 0.14*	−0.63 ± 0.10*	Mm, Ac, Ap
CCL3	−0.98 ± 0.06	Serum:	−2.05 ± 0.03*	−1.25 ± 0.09*	−1.01 ± 0.09*	Mm, Ac, Ap
		Tissue:	−0.93 ± 0.01*	−0.95 ± 0.01*	−0.94 ± 0.06*	Mm, Ac, Ap
CCL5	−0.90 ± 0.07	Serum:	−0.78 ± 0.03*	Not detected	0.33 ± 0.32	Mm
		Tissue:	−0.90 ± 0.16*	0.34 ± 0.13	0.07 ± 0.27	Mm
TNFα	−1.10 ± 0.06	Serum:	−1.36 ± 0.38*	−2.15 ± 0.01*	−1.09 ± 0.17*	Mm, Ac, Ap
		Tissue:	−1.14 ± 0.10*	−0.93 ± 0.01*	−1.21 ± 0.03*	Mm, Ac, Ap
IFNγ	−0.79 ± 0.10	Serum:	−0.60 ± 0.16*	−1.48 ± 0.72*	−1.21 ± 0.22*	Mm, Ac, Ap
		Tissue:	−0.81 ± 0.31*	−0.72 ± 0.05*	−0.84 ± 0.05*	Mm, Ac, Ap
CXCL1	−1.20 ± 0.02	Serum:	−1.15 ± 0.27*	Not detected	Not detected	Mm
		Tissue:	−1.11 ± 0.05*	Too few points &	−1.15 ± 0.29*	Mm, Ap

This was used to determine which species and source comparisons could be made for each cytokine in the Comparison column.

Slopes in italics are not different from zero ($P > 0.05$ for regression test).

*Denotes slope is similar to the standard and can be reliably quantified.

&Denotes values are below the assay's lower limit of detection.

^Denotes values are above the assay's upper limit of quantification.

transitional group between Mm-UKY and Mm-Wild for TNFα and IL-4 (**Figure 2**). Heightened concentrations of IL-6, TNFα, and IL-4 support previous pathogen exposure and a possibility of current infection (52, 53). Thus, Mm-Kenya, Mm-Wild, and Ap had a relatively activated immune system, while Mm-UKY and Ac possessed a more naïve immune system (54). There were no consistent differences between regenerators and non-regenerators when comparing serum cytokine concentrations from uninjured animals (**Figure 2**).

Next, we quantified the systemic injury response for each cytokine compared to its baseline, beginning 24 h (D1) after injury and over the next 20 days (**Figure S2A**). In most cases (except IL-2, IL-6, IL-17, and CXCL1), there was no effect of day (**Table S3**), indicating that the immediate systemic response persisted for 20 days. Animals with a more naïve immune system showed increased IL-2 and TNFα, and decreased IL-1α compared to a relatively activated immune system (**Figure S2A**:

solid lines compared to intermittent lines and **Data File S1**). Regenerating animals (*Acomys spp.*) showed decreased IL-5, IL-6, IL-17, CCL3, and CXCL1 compared to *M. musculus* undergoing fibrotic repair (**Figures S2A,B**: red lines compared to black lines and **Data File S1**). This latter result supported that animals healing by fibrotic repair and regeneration could be separated by their systemic response to injury.

A Regenerative Microenvironment Is Marked by Induction of T Cell-Associated Cytokines and a Dampened Pro-inflammatory Cytokine Response

Resident cells and infiltrating immune cells secrete cytokines that likely polarize the injury microenvironment to support regeneration or fibrotic repair (11, 12, 15, 16, 18, 23, 55). Thus, to quantify local cytokine concentrations we assayed tissue

TABLE 2 | Comparison of *A. cahirinus* predicted peptide sequences used in cytokine analysis.

Gene ID	Peptide ID	% similar to *M. musculus*	% similar to *R. norvegicus*	% similar to *H. sapiens*
Il1a	IL-1α	82.90	86.90	66.90
Il1b	IL-1β	87.71	87.71	72.35
Il2	IL-2	70.41	84.61	71.59
Il4	IL-4	66.45	77.21	56.32
Il5	IL-5	90.15	84.84	68.93
Il6	IL-6	75.23	78.97	48.13
Il10	IL-10	85.05	87.93	74.13
Il12a	IL-12 p35	70.42	80.54	55.25
Il12b	IL-12 p40	73.58	74.10	63.33
Il17a	IL-17	84.88	83.13	75.58
Cxcl1	KC	80.37	81.30	69.15
Ccl2	MCP-1	73.50	70.86	43.70
Ccl3	MIP-1α	93.54	94.62	81.72
Ccl5	RANTES	88.04	84.78	85.86
Csf2	GM-CSF	65.24	73.75	61.70
IFNγ	IFNγ	56.77	57.05	41.56
Tnf	TNFα	95.81	96.65	84.93

*Alignments are supplemental (**Data File S2**).*
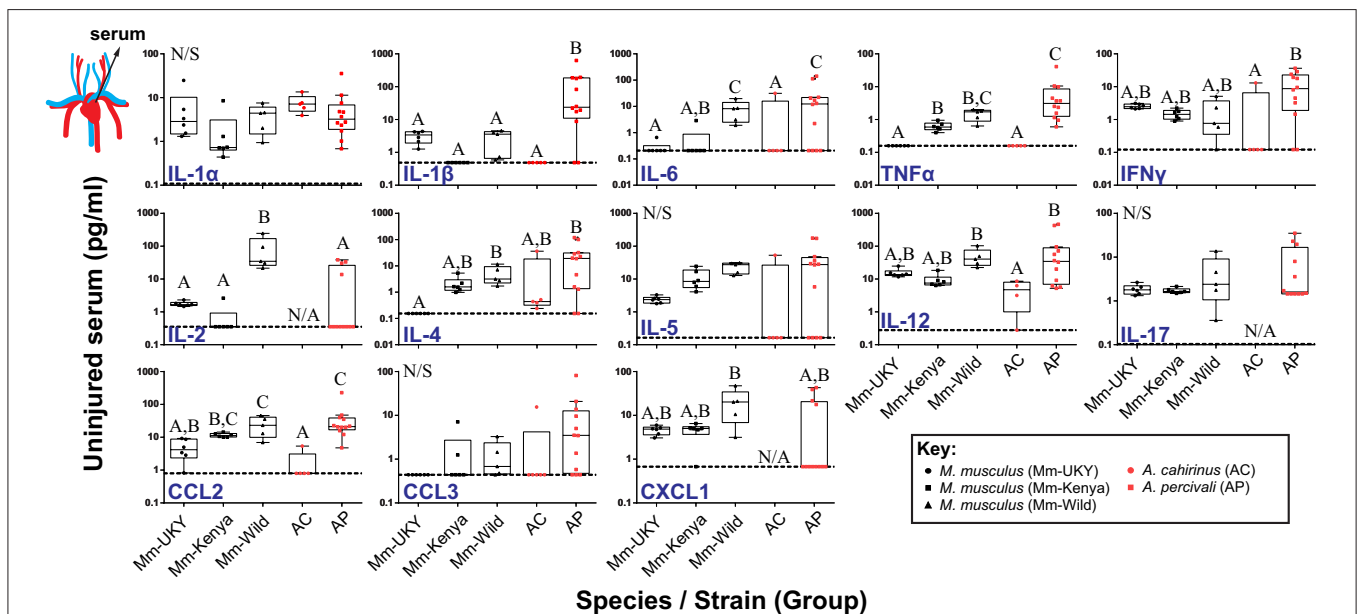
FIGURE 2 | Regenerative ability and immune status are associated with a distinct systemic immune response to injury. Comparison of cytokine concentrations in serum from uninjured animals showed higher concentrations of IL-4, IL-6, CCL2, and TNFα in wild-caught animals compared to laboratory-reared animals indicating that wild animals have a "primed" immune system. No difference was found between non-regenerators (Mm-UKY, Mm-Kenya, and Mm-Wild) (black points) and regenerators (Ac and Ap) (red points) for systemic changes the cytokines examined. Data represent box and whiskers with median, interquartile range and individual data points. N/A denotes concentrations could not be quantified in any animal of the group. The dashed line in each graph represents the lower limit of detection for the specific cytokine. N/S denotes $P > 0.05$ for One-way ANOVA (See **Table S2**) and different letters above the data denotes $P \leq 0.05$ for Tukey-Kramer pairwise comparisons (See **Data File S1**). Data represent mean and S.E.M. for at least $n = 5$ animals per species per timepoint. The cartoon circulatory system indicates that the measured values were from serum.

lysate collected throughout the healing response (**Figure 1B**). IL-1α could not be compared because baseline concentrations were above the upper limit of quantification in more than 80% of samples, indicating that IL-1α in the ear pinna was at

least two orders of magnitude greater than the other cytokines measured. Although ear pinna tissue is structurally similar across species (41), local cytokines in *Acomys* were consistently detected at lower concentrations compared to *M. musculus*. Moreover,

because the concentration of a particular cytokine may not be as important as the dynamic response of that cytokine, we compared the change in cytokine concentration compared to baseline over 20 days (**Figure 3** and **Figure S2B**). Injury elicited significant changes over time compared to baseline for all cytokines measured in tissue lysate supporting a dynamic response (**Table S4**). Furthermore, while most cytokines shared similar trajectories over time, there was an effect of Group and the Group*Day interaction for all cytokines supporting significant differences in the magnitude of change among the groups (**Figure 3**, **Figure S2B** and **Table S4**). Supporting an inflammatory response in all groups, several pro-inflammatory cytokines (IL-6, TNFα) and myeloid chemotactic factors (CCL3, CSF2, and CXCL1) showed an increase compared to baseline between D1 and D3 that then decreased to baseline or below between D5 and D20 (**Figure S2B**). There was also an overall decrease compared to baseline for IL-5 and a small but significant change from baseline for IL-2 and IL-4 across all groups (**Figure S2B**). Animals with naïve immune responses had a stronger increase in CCL3 and a smaller increase for CCL2 and CXCL1 compared to activated immune responses (**Figure S2B**: solid compared to intermittent lines). We also identified several cytokines that showed differential changes between regeneration and fibrotic repair that we describe below (**Figure 3** and **Figure S2B**: red compared to black lines).

During the acute inflammatory phase (D1 and D2), CCL2 and CXCL1 were increased 9 and 12-fold during fibrotic repair compared to regeneration, respectively (**Figure 3**). IL-6 showed a similar result at D2 where Mm-UKY, Mm-Kenya and Mm-Wild were increased 10-fold compared to Ac and Ap (**Figure 3**). Additionally, IL-17 was increased in Ap, but decreased in Mm-UKY and Mm-Kenya and IL-12 was increased in Ap compared to all *Mus* (**Figure 3**). Interestingly, the TNFα response—a biomarker of inflammation—could not reliably separate fibrotic repair and regeneration (**Figure 3**).

Regardless of healing outcome, re-epithelialization occurs by D10 (41, 42) coincident with resolution of many pro-inflammatory cytokine responses (**Figures S2A,B**: yellow bars). While there were some differences among groups for the timing of resolution, IL-1β, TNFα, and CCL2 were similar to or below baseline at D10 for all species (**Figure 3**). IL-6 also followed this pattern; however, there was a differential response where Ac remained elevated through D20 while all other animals decreased below baseline (**Figure 3**).

At D20, during tissue morphogenesis, the only cytokines that showed a differential response were IL-12 and IL-17 that were increased during regeneration compared to fibrotic repair, although IL-17 was only increased in wild Ap (**Figure 3**). The anti-inflammatory cytokine IL-4 did not differ over time with respect to regenerative ability, suggesting that the differences in pro-inflammatory cytokine release are likely not an IL-4 mediated response. Our results suggest that subtle differences in how cytokines are deployed in the injury microenvironment can distinguish regeneration or fibrotic repair. These data suggested that strong, acute increases in the pro-inflammatory cytokines IL-6, CCL2, and CXCL1 were associated with fibrosis, while the release of IL-12 and IL-17 during new tissue formation was associated with regeneration.

Regeneration Is Associated With an Early Burst of T Cell Influx to the Injury Site

The release of IL-12 and IL-17 into the regenerative microenvironment suggested enhanced T cell activation during regeneration (56, 57). Therefore, we quantified T cell influx into uninjured and healing tissue from our laboratory populations of *Mus* (Mm-UKY) and *Acomys* (Ac) using flow cytometry with an antibody to the extracellular portion of the T cell marker CD3. We observed significant differences in CD3+ cells in injured tissue between species over time (two-way ANOVA, $n = 57$; species: Df = 1, $F = 49.49$ $P < 0.001$; day: Df = 6, $F = 89.07$, $P < 0.001$; species*day: Df = 6, $F = 21.49$ $P < 0.001$) (**Figure 4A**). In uninjured tissue, Mm-UKY had 10-times more CD3+ cells compared to Ac (Tukey-Kramer HSD *post-hoc* test, Df = 6, $t = 6.21$, $P < 0.001$) (**Figure 4A**). While the total number of CD3+ cells that infiltrated the wound was higher in Mm-UKY compared to Ac, there was a greater fold change relative to D0 for CD3+ cells during regeneration compared to fibrotic repair (**Figure 4B**). Ac exhibited a monophasic response to injury starting on D1 with a 78-fold influx of T cells that peaked on D3 and remained above baseline at D15. Mm-UKY showed a biphasic response with peak influx of 10-fold at D7 that returned to baseline at D15 (**Figure 4B**). Importantly, at D15, when IL-12 was increased (**Figure 3**), the influx of CD3+ cells remained high in Ac compared to Mm-UKY (**Figure 4B**).

We next used immunohistochemistry with an antibody specific to the intracellular portion of the CD3 receptor to assess the spatial distribution of T cells during acute inflammation and morphogenesis (**Figures 4C–E**). In Mm-UKY most CD3+ cells were associated with the epidermis and were rarely observed distal to the amputation plane (**Figure 4C**). On the other hand, CD3+ cells in Ac were present in the epidermis and dermis, and regularly observed in healing tissue distal to the amputation plane (**Figure 4E**). At D15, CD3+ cells were found in the epidermis and dermis of both species (**Figures 4D,F**). Interestingly, CD3+ cells associated with the epidermis in Mm-UKY (**Figure 4G**) exhibited a spindle-shape morphology compared to a rounded shape in Ac (**Figure 4H**). There also appeared to be more CD3+ cells in the dermis of Ac compared to Mm-UKY (**Figures 4D,F**), and the CD3+ cells tended to localize near regenerating hair follicles in Ac (**Figure 4I**). Attempts to characterize individual T cell phenotypes during regeneration using flow cytometry and IHC using 19 commercially available antibodies were unsuccessful and supported significant differences in antibody-epitope binding between species that prevented further T cell phenotyping by receptor subtype in *Acomys* (**Table S6**). Therefore, we interrogated a comparative injury RNAseq dataset for differential expression of T cell associated transcripts between *Mus* and *Acomys* (41). While expression for genes associated with non-lymphocyte immune cell populations were generally similar between species, several transcripts associated with T cells and natural killer cells were increased in *Acomys* and decreased in *Mus* in response to injury (**Figure 4J**). Increased expression
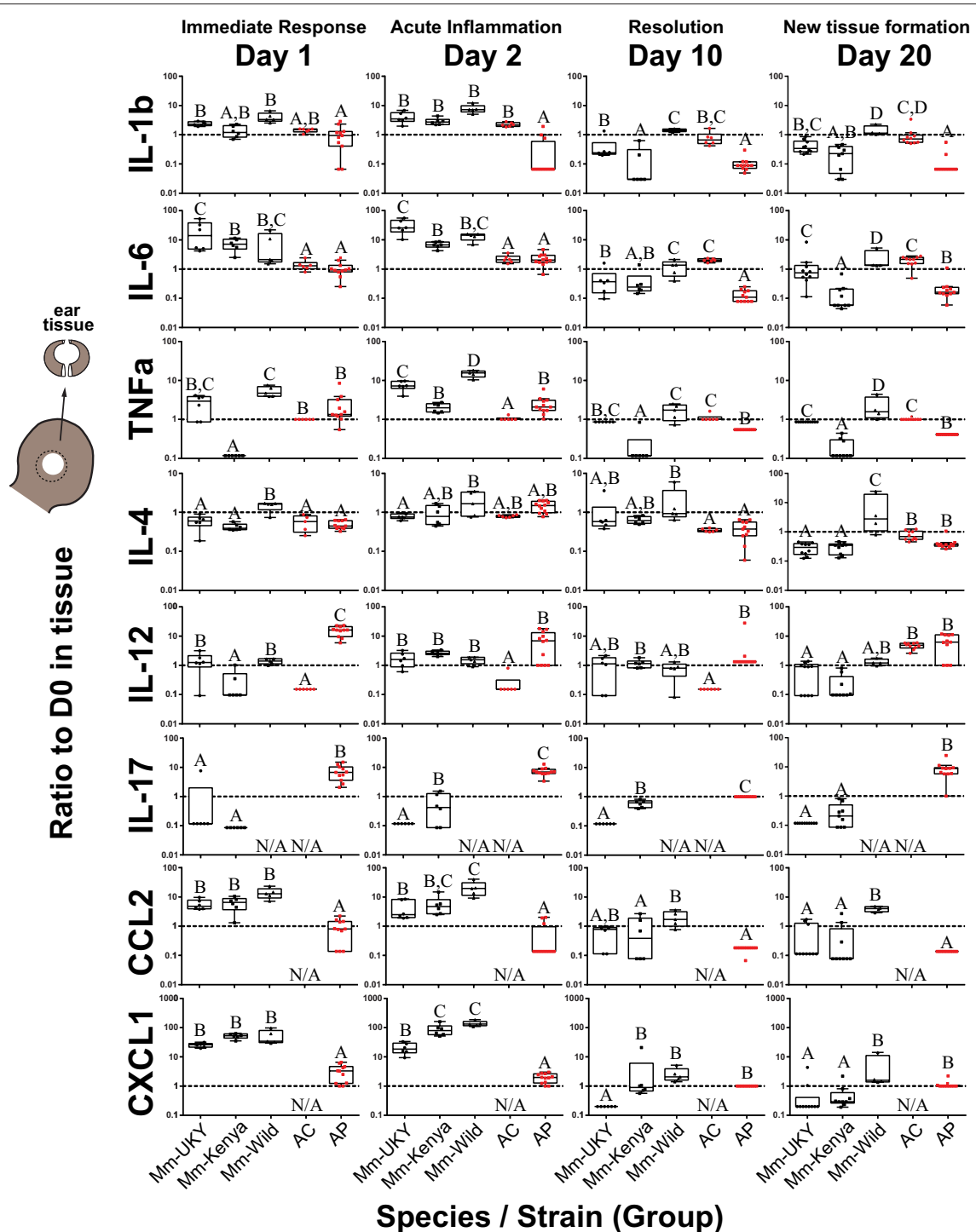
FIGURE 3 | Injury-induced cytokine concentrations are dynamic in the tissue microenvironment with acute increases in IL-6, CCL2 and CXCL1 strongest in non-regenerating animals. Cytokine ratios present in tissue lysate relative to D0 at D1, 2, 10, and 20 days post ear punch injury. Non-regenerators (Mm-UKY, Mm-Kenya, and Mm-Wild: Black) show a stronger response compared to regenerators (Ac and Ap: Red) for IL-6, CCL2, and CXCL1 during the acute inflammatory phase. These differences mostly resolved by D10. In contrast, regenerators showed a stronger IL-12 and IL-17 response during tissue morphogenesis. Data represent box and whiskers with median, interquartile range and individual data points. N/A denotes concentrations could not be quantified. The dashed line at Y = 1 represents no change compared to D0. Each graph showed $P < 0.05$ for a group effect using a One-way ANOVA on log-transformed data (See **Table S5**) and different letters above each group denotes $P < 0.05$ for Tukey-Kramer pairwise comparisons (See **Data File S1**).
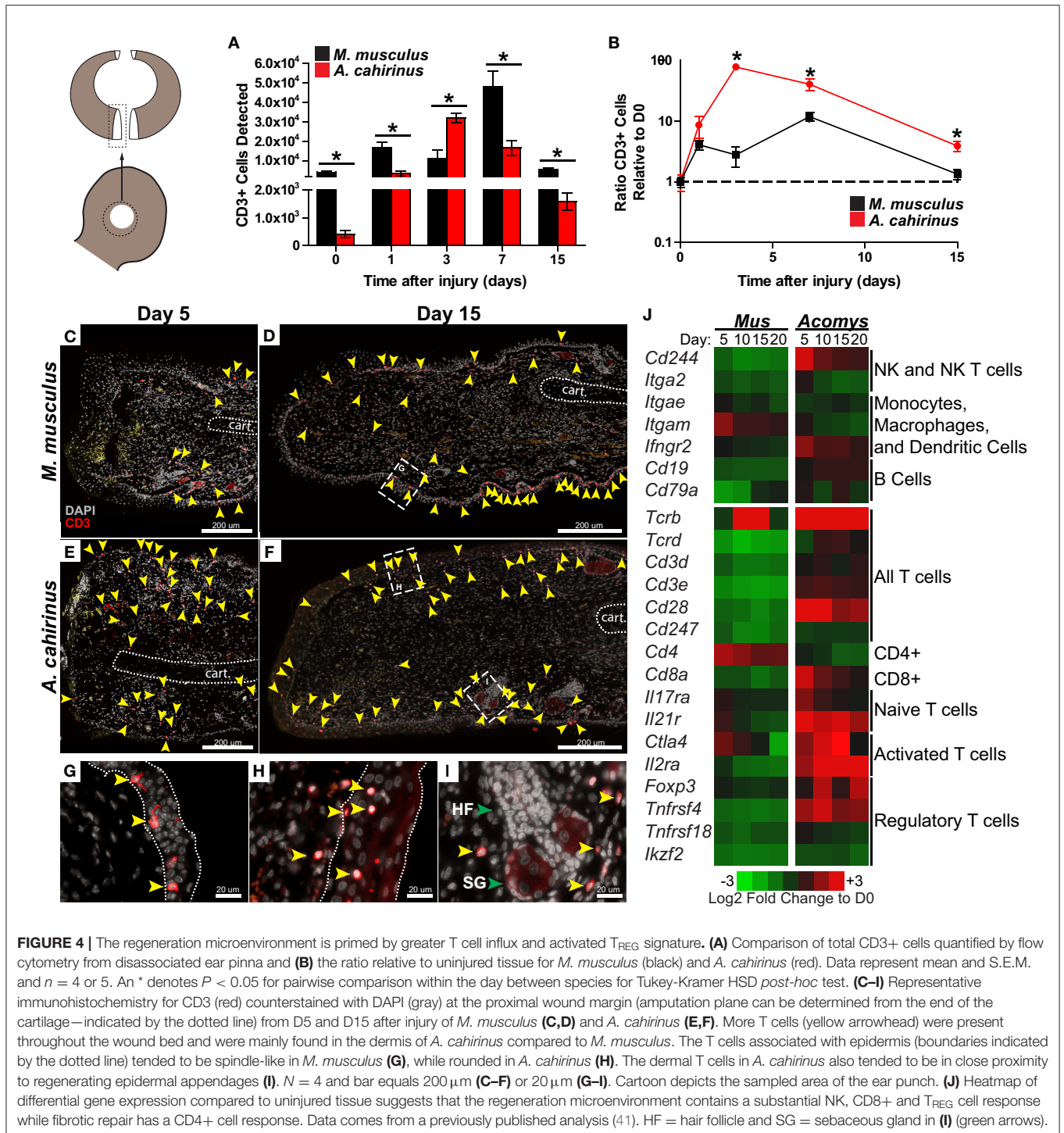
FIGURE 4 | The regeneration microenvironment is primed by greater T cell influx and activated T_{REG} signature**. (A)** Comparison of total CD3+ cells quantified by flow cytometry from disassociated ear pinna and **(B)** the ratio relative to uninjured tissue for *M. musculus* (black) and *A. cahirinus* (red). Data represent mean and S.E.M. and $n = 4$ or 5. An * denotes $P < 0.05$ for pairwise comparison within the day between species for Tukey-Kramer HSD *post-hoc* test. **(C–I)** Representative immunohistochemistry for CD3 (red) counterstained with DAPI (gray) at the proximal wound margin (amputation plane can be determined from the end of the cartilage—indicated by the dotted line) from D5 and D15 after injury of *M. musculus* **(C,D)** and *A. cahirinus* **(E,F)**. More T cells (yellow arrowhead) were present throughout the wound bed and were mainly found in the dermis of *A. cahirinus* compare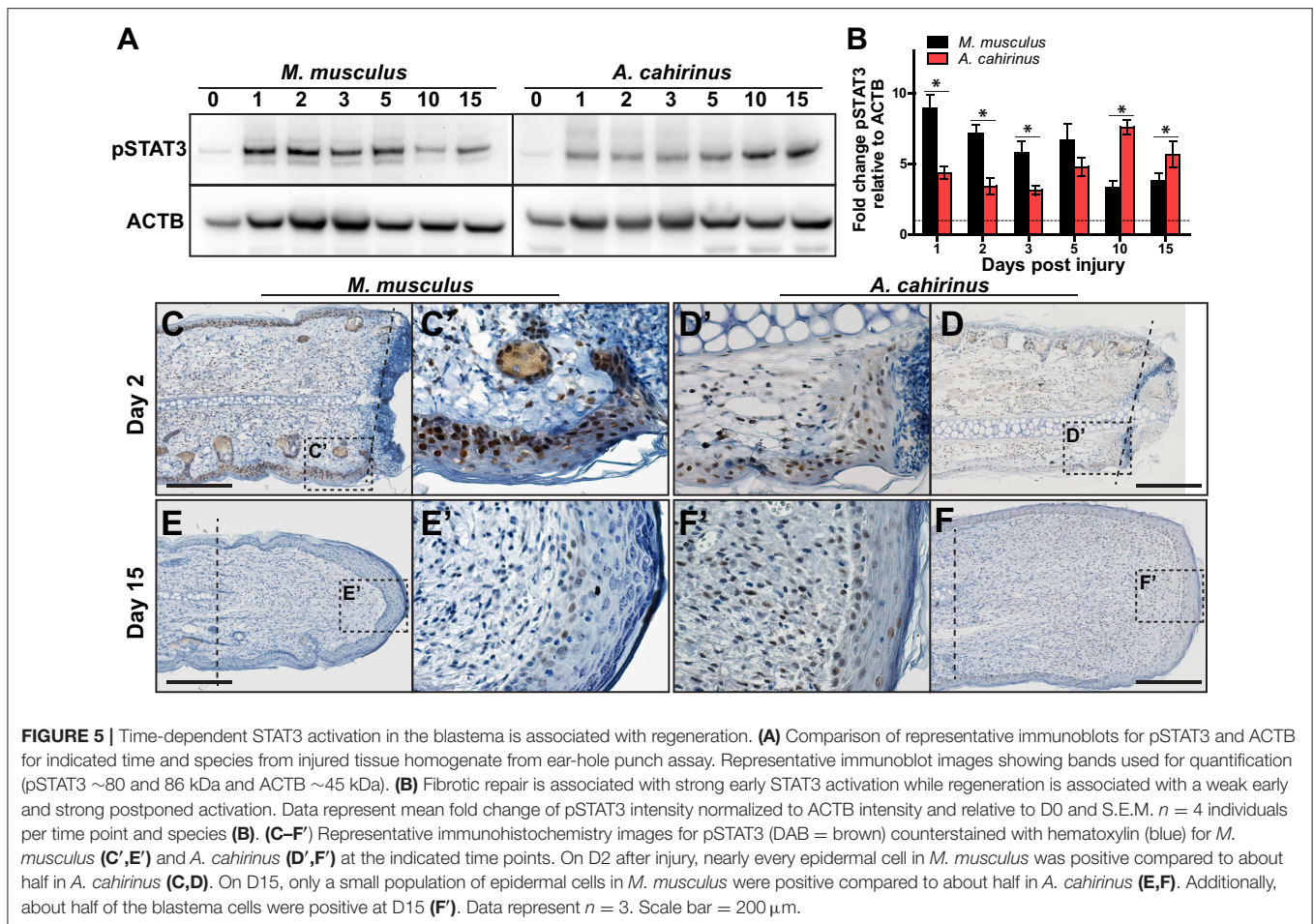d to *M. musculus*. The T cells associated with epidermis (boundaries indicated by the dotted line) tended to be spindle-like in *M. musculus* **(G)**, while rounded in *A. cahirinus* **(H)**. The dermal T cells in *A. cahirinus* also tended to be in close proximity to regenerating epidermal appendages **(I)**. $N = 4$ and bar equals 200 μm **(C–F)** or 20 μm **(G–I)**. Cartoon depicts the sampled area of the ear punch. **(J)** Heatmap of differential gene expression compared to uninjured tissue suggests that the regeneration microenvironment contains a substantial NK, CD8+ and T_{REG} cell response while fibrotic repair has a CD4+ cell response. Data comes from a previously published analysis (41). HF = hair follicle and SG = sebaceous gland in **(I)** (green arrows).

of *Cd8*, *Ctla4*, *Il2ra*, *Foxp3*, and *Tnfrsf4* specifically suggested an activated cytotoxic and regulatory T cell response during regeneration but not fibrotic repair (**Figure 4J**). During fibrotic repair, *Cd4* was differentially increased at D5 and D10 suggesting the presence of CD4 helper T cells not present during regeneration (**Figure 4J**). Together, these data demonstrate that regeneration was associated with a proportionally greater influx of CD3+ cells that accumulate quickly at the injury site and that

specific subtypes of activated T cells were preferentially associated with regeneration.

STAT3 Is Activated Independently From IL-6 During Blastema Formation

We also sought to test our observation that strong induction of the pro-inflammatory cytokine IL-6 was associated with the acute inflammatory phase of fibrotic repair. To do this, we assayed

FIGURE 5 | Time-dependent STAT3 activation in the blastema is associated with regeneration. **(A)** Comparison of representative immunoblots for pSTAT3 and ACTB for indicated time and species from injured tissue homogenate from ear-hole punch assay. Representative immunoblot images showing bands used for quantification (pSTAT3 ~80 and 86 kDa and ACTB ~45 kDa). **(B)** Fibrotic repair is associated with strong early STAT3 activation while regeneration is associated with a weak early and strong postponed activation. Data represent mean fold change of pSTAT3 intensity normalized to ACTB intensity and relative to D0 and S.E.M. $n = 4$ individuals per time point and species **(B)**. **(C–F′)** Representative immunohistochemistry images for pSTAT3 (DAB = brown) counterstained with hematoxylin (blue) for *M. musculus* **(C′,E′)** and *A. cahirinus* **(D′,F′)** at the indicated time points. On D2 after injury, nearly every epidermal cell in *M. musculus* was positive compared to about half in *A. cahirinus* **(C,D)**. On D15, only a small population of epidermal cells in *M. musculus* were positive compared to about half in *A. cahirinus* **(E,F)**. Additionally, about half of the blastema cells were positive at D15 **(F′)**. Data represent $n = 3$. Scale bar = 200 μm.
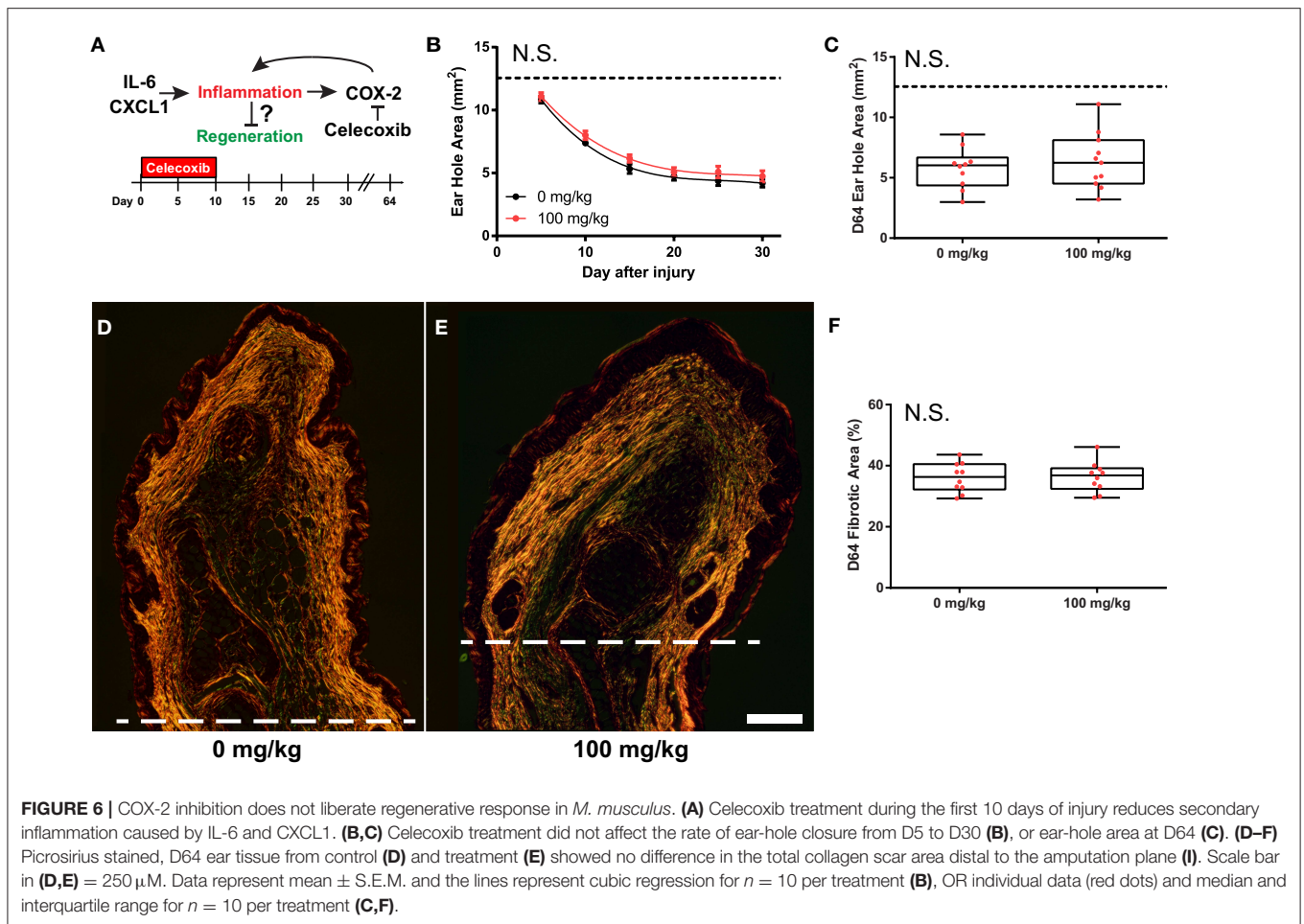
for IL-6 signaling using STAT3 phosphorylation (**Figures 5A–F**). STAT3 is phosphorylated in response to the ligand IL-6 binding its membrane receptor, which activates signal transduction in target cells (58). Corroborating our ELISA quantification for IL-6 in the tissue microenvironment, we found that pSTAT3 increased 8-fold in response to injury in Mm-UKY during the acute inflammatory phase (**Figures 5A,B**). Similarly, during fibrosis when IL-6 concentrations resolved in Mm-UKY, pSTAT3 began to decline toward baseline (**Figures 5A,B**). In *Acomys*, pSTAT3 was significantly elevated at D1, although to a lesser extent than compared to Mm-UKY (**Figures 5A,B**). Moreover, during blastema formation and new tissue formation (D10-15) when our ELISA data showed increased IL-6 compared to baseline in Ac (**Figure 3**), analysis of pSTAT3 showed further induction of pSTAT3 in Ac (**Figures 5A,B**).

To determine the cellular localization of STAT3 phosphorylation, we assayed for pSTAT3 using immunohistochemistry during the acute inflammatory phase (D2) and new tissue formation (D15) (**Figures 5C–F**). Supporting the immunoblot data, both species showed extensive nuclear staining for pSTAT3 at D2 in the epidermis and mesenchymal compartments (**Figures 5C′,D′**). Positive staining in the epidermis > 200 μM proximal to the amputation plane

suggested STAT3 activation was a pervasive response to injury within the ear pinna in both species (**Figures 5C,D**). Supporting the 2-fold difference in pSTAT3 observed between Mm-UKY and Ac (**Figures 5A′,B′**), we found that nearly every epidermal cell in Mm-UKY appeared positive for pSTAT3 whereas less than half of the epidermal cells were positive in Ac (**Figures 5C,D**). The internal tissue compartments (e.g., dermis, cartilage, muscle and adipose) at D2 were similar between species with approximately half of the total cells positive for pSTAT3. At D15, only a few pSTAT3 positive cells were present in Mm-UKY and they were isolated to the epidermis distal to the amputation plane (**Figures 5E,E′**). In contrast, pSTAT3 positive cells were widespread throughout the blastema in Ac (**Figures 5F,F′**). Together, these data support stronger IL-6 mediated STAT3 activation in Mm-UKY compared to Ac during the acute inflammatory phase and increased STAT3 activation during blastema formation.

Greater increases in IL-6 and CXCL1 during the acute inflammatory phase of fibrotic repair in *M. musculus* suggested that these molecules might antagonize a potential regenerative response. Previous studies have shown that a balance in these molecules regulate wound healing as IL-6 and CXCL1 are potent pro-inflammatory molecules and hyper-elevated

FIGURE 6 | COX-2 inhibition does not liberate regenerative response in *M. musculus*. **(A)** Celecoxib treatment during the first 10 days of injury reduces secondary inflammation caused by IL-6 and CXCL1. **(B,C)** Celecoxib treatment did not affect the rate of ear-hole closure from D5 to D30 **(B)**, or ear-hole area at D64 **(C)**. **(D–F)** Picrosirius stained, D64 ear tissue from control **(D)** and treatment **(E)** showed no difference in the total collagen scar area distal to the amputation plane **(I)**. Scale bar in **(D,E)** = 250 µM. Data represent mean ± S.E.M. and the lines represent cubic regression for *n* = 10 per treatment **(B)**, OR individual data (red dots) and median and interquartile range for *n* = 10 per treatment **(C,F)**.
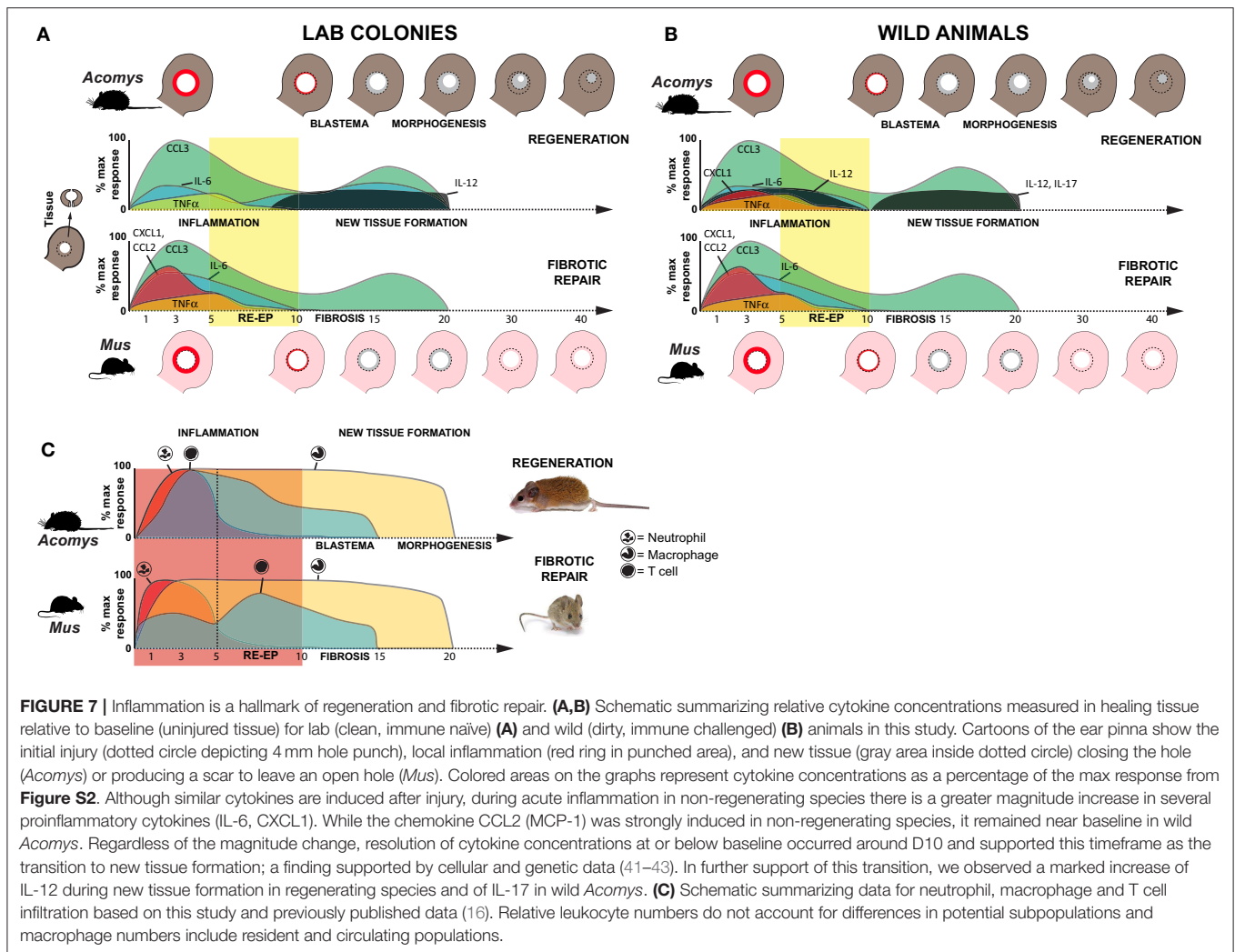
concentrations after injury are attributed to aberrant healing and chronic inflammation (59–61). Additionally, genetic ablation of *IL-6*, the *IL-6 receptor*, or the *CXCL1 receptor* (*CXCR2*), causes severely delayed re-epithelialization, scab formation and abhorrent wound healing in cutaneous and incisional wounds (62–65). IL-6 signaling activates several downstream mediators of inflammation including cyclooxegenase-2 (COX-2), and its enzymatic products can amplify the inflammatory response (66). To test if COX-2 activity promotes fibrosis in the ear pinna, we used our ear punch assay in Mm-UKY healing tissue treated with Celecoxib, a specific and potent COX-2 inhibitor (67) (**Figure 6A**). Comparing ear-hole closure between celecoxib- and vehicle-treated animals there was no support for a difference in the rate of closure (D5 through D30) (repeated measures two-way ANOVA, *n* = 31; treatment: Df = 1, *F* = 2.42, *P* = 0.137; day: Df = 5, *F* = 179.62, *P* < 0.001; treatment*day: Df = 5, *F* = 0.36, *P* = 0.875) (**Figure 6B**). Similarly, only one out of five celecoxib-treated animals had not completed re-epithelialization by D10. Comparison of ear-hole area at D64 showed no support for a difference between treatment and control ears (unpaired *t*-test; *t* = 0.671, *P* = 0.512) (**Figure 6C**). Lastly, while the intensity of Picrosirius stain appeared to be lower in celecoxib treated animals compared to controls, there was no difference

in the area of collagen deposition at D64 (unpaired *t*-test, *t* = 0.104, *P* = 0.918) (**Figures 6D–F**). Thus, these data support that systemic inhibition of COX-2 activity is not sufficient to reduce fibrosis or induce a regenerative response after ear pinna injury in *M. musculus*.

DISCUSSION

In this study, we performed a temporal cytokine characterization of the immune response where identical injuries in closely related species underwent two different healing responses: regeneration or fibrotic repair. Importantly, our experimental design also leveraged a comparison of animals with an activated (wild-caught) or naïve (lab bred) immune system in order to identify species-specific cytokine changes that were associated with regeneration and not due to an environment-immunity interaction (**Figures 7A–C**). Our analyses showed that regardless of healing outcome, injury induced a common set of pro-inflammatory factors (IL-6, and TNFα) and chemokines (CCL3, CSF2, and CXCL1) during the acute inflammatory phase of healing. While this supports that some measure of inflammation occurs early during fibrotic repair and regeneration, we did find significantly greater responses for IL-6, CCL2, and

FIGURE 7 | Inflammation is a hallmark of regeneration and fibrotic repair. **(A,B)** Schematic summarizing relative cytokine concentrations measured in healing tissue relative to baseline (uninjured tissue) for lab (clean, immune naïve) **(A)** and wild (dirty, immune challenged) **(B)** animals in this study. Cartoons of the ear pinna show the initial injury (dotted circle depicting 4 mm hole punch), local inflammation (red ring in punched area), and new tissue (gray area inside dotted circle) closing the hole (*Acomys*) or producing a scar to leave an open hole (*Mus*). Colored areas on the graphs represent cytokine concentrations as a percentage of the max response from **Figure S2**. Although similar cytokines are induced after injury, during acute inflammation in non-regenerating species there is a greater magnitude increase in several proinflammatory cytokines (IL-6, CXCL1). While the chemokine CCL2 (MCP-1) was strongly induced in non-regenerating species, it remained near baseline in wild *Acomys*. Regardless of the magnitude change, resolution of cytokine concentrations at or below baseline occurred around D10 and supported this timeframe as the transition to new tissue formation; a finding supported by cellular and genetic data (41–43). In further support of this transition, we observed a marked increase of IL-12 during new tissue formation in regenerating species and of IL-17 in wild *Acomys*. **(C)** Schematic summarizing data for neutrophil, macrophage and T cell infiltration based on this study and previously published data (16). Relative leukocyte numbers do not account for differences in potential subpopulations and macrophage numbers include resident and circulating populations.

CXCL1 during fibrotic repair. In contrast, regeneration was uniquely associated with local increases in IL-12 and IL-17 during new tissue formation, although increased IL-17 was only detected in wild *Acomys*. Regeneration was associated with a stronger influx of T cells during acute inflammation that was closely associated with the dermis during blastema formation. Comparative gene expression analysis supported a bias toward activated and regulatory T cells among these populations. This latter point suggests that T cells may be responding to different inflammatory cues present in the wound microenvironment that bias their phenotype to support or direct tissue morphogenesis in spiny mice. This hypothesis awaits further functional assessment of specific T cell populations.

Recent studies comparing immune profiles between laboratory-reared and pet-store or wild-caught *M. musculus* demonstrated that non-laboratory strains have more CD44$^+$ effector T cells, memory T cells and circulating neutrophils (68, 69). The elevated baseline concentrations of IL-4, IL-6, CCL2, and TNFα that we measured in circulation from uninjured, immune-challenged animals support larger active

populations of effector and memory T cells. These data reinforce that our immune-challenged group had been exposed to more pathogens than the laboratory-reared mice which is undoubtedly the case. In addition to the increased baseline concentrations of these cytokines, we also found significant differences in the response to injury for IL-1α and TNFα between animals with an activated vs. naïve immune system. Studying wild-caught populations enabled us to identify responses that accurately reflected phenotypic differences between species, rather than differences that could be explained by immune status. Of particular importance was our inclusion of wild-caught *A. percivali* that indicate increases in TNFα, CCL2, and CXCL1 are not inhibitory to regeneration, although the magnitude of increase in *Mus* was still significantly higher (**Figures 7A,B**). Additionally, we observed high variation in cytokine concentrations across our dataset indicating that the immune response to injury could be confounded by individual variation. Ultimately, however, our data support injury eliciting a specific cytokine response that is independent of baseline immune status which affects the timing of events but does not change healing outcome.

Acute inflammation is a necessary component of the innate immune reaction and occurs in response to leukocyte recruitment and the activation of local myeloid and lymphoid cells. Regardless of healing outcome, our data demonstrate an acute inflammatory response that resolves within ~10 days; a timeframe in line with human and rodent wound healing studies (7, 70). During inflammation in *Mus* (wild and lab) and wild *Acomys*, we found the local release of CCL3, CSF2, IL-6, TNFα, and CXCL1, which are known to be potent chemokines for monocytes, macrophages and neutrophils (**Figures 7A,B** and **Figure S2**). That CSF2 and CXCL1 were not consistently detected in laboratory reared *Acomys* suggests that production of these cytokines is more reflective of immune, rather than healing status. Moreover, the local release of IL-6 and TNFα supports the presence of activated macrophages and neutrophils as a common injury response (**Figure 7C**). However, our results did reveal that IL-6, CCL2, and CXCL1 were significantly more enriched within mouse tissue during the inflammatory period (**Figures 7A,B** and **Figure S2**). The differential increase in these cytokines is consistent with our previous work showing that neutrophils infiltrate injured spiny mouse tissue slower compared to laboratory mice (16). They are also in line with a report from spiny mouse skin regeneration which found lower concentrations of similar pro-inflammatory cytokines (23). IL-6, CXCL1 and CCL2 are known to positively regulate the speed of re-epithelialization (62–64), which we find to be delayed at most 5 days in *A. cahirinus* compared to *M. musculus* (41).

In addition to the magnitude increase in IL-6 and CXCL1, we found that increased local CCL2 was specific to fibrotic repair. CCL2 was first identified as a monocyte-specific chemoattractant to sites of injury and infection, although its activity appears to be far more pleiotropic (71, 72). CCL2 also attracts neutrophils and supports neutrophil-dependent tissue damage (71). As such, the amount of CCL2 that is released into an injury microenvironment regulates the healing response and studies support there is a positive relationship between CCL2 and the amount of fibrosis during fibrotic repair (73–75). However, a careful balance must be maintained as CCL2 knockout mice do not heal wounds (76). Thus, it is possible that the reduced IL-6, CCL2, and CXCL1 responses are responsible for reduced fibrosis in spiny mice. Although these key factors appear to interact in the hierarchy of the progression of fibrotic repair, the paracrine mechanism of how they would activate dermal fibroblasts remains unknown. It is likely another cell-type, such as macrophages or T cells, is mediating the signal.

Injured tissues contain tissue specific macrophages (derived from yolk sac precursors) and infiltrating macrophage precursors (monocytes) recruited from the bone marrow and systemic circulation. Not only do these two macrophage populations secrete cytokines into the wound environment, but they actively respond to cytokines and growth factors which alters their phenotype [reviewed in (77)]. Macrophages are required for normal wound healing (26, 28, 78) and similarly required for complex tissue regeneration (11, 13, 16, 79). Because macrophages, like many immune cells, exhibit phenotypes that are context dependent, there is an increasing appreciation that

specific macrophage populations may regulate the magnitude and type of healing response (80). Supporting this hypothesis, previous work in spiny mice revealed that macrophage infiltration and accumulation was similar between lab mice and spiny mice following ear punch injury (16). While unique macrophage phenotype may exist in spiny mice, it is equally plausible that the unique combination of cytokines expressed in the evolving wound environment create macrophage population dynamics that are specific to regeneration or fibrotic repair. For instance, CCL2 is a potent macrophage driver that can act singly or synergistically to polarize macrophages and affect production of secreted products [reviewed in (81)]. Resolving which specific macrophage populations are present, and how they behave during regeneration and fibrotic repair, will require single-cell approaches and thus awaits further exploration.

Extending our observation that the IL-6 response was weaker during regeneration compared to fibrotic repair, we found diminished activation of STAT3 during acute inflammation (D1-10) in spiny mouse epidermis compared to mouse. Interestingly, we observed an increase in pSTAT3 during blastema formation, whereas the amount of pSTAT3 declined during fibrotic repair. Furthermore, during new tissue formation at D15 many blastemal cells were STAT3 positive. Given that IL-6 concentrations did not appreciably increase during blastema formation or tissue morphogenesis the increase in STAT3 activity is likely independent of IL-6. STAT3 is activated through multiple pathways (e.g., leukemia inhibitory factor, epidermal growth factor, palette derived growth factor, IL-10, IL-17, etc.). Although IL-17 increased in *A. percivali* after D10, it did not increase in *A. cahirinus* suggesting it is not responsible for the late phase of STAT3 phosphorylation. Given that STAT3 signaling is multifaceted, one potential biological link is that STAT3 activity is necessary for satellite-cell activation and axon regeneration in mammals (82–84). Interestingly, the expression of *Sal4*—a factor necessary for blastema maintenance in *Xenopus* and *Ambystoma*—is regulated by pSTAT3 (85–87). While *Sal4* does not have a mammalian homolog, this data supports that activation of STAT3 in regenerating tissue is an evolutionary conserved mechanism and interrogating unique STAT3 targets in spiny mice may uncover mechanisms that regulate blastema formation in mammals.

Inhibition of downstream signaling induced by IL-6 / CXCL1, such as arachidonic acid metabolism by COX-2, has been shown to reduce fibrosis post epidermal injury (e.g., incisional, cutaneous and chronic pressure wounds) (88–90). Celecoxib treatment to inhibit COX-2 in the present study may have slowed re-epithelialization. Additionally, while the total area of fibrosis was not different between celecoxib- and vehicle-treated animals there appeared to be a small reduction in the total amount of collagen produced in celecoxib-treated animals from reduced intensity of picrosirius staining. However, similar to previous reports, reduction in COX-2 activity did not induce regeneration, supporting that inflammation is not the ultimate inhibitory barrier.

In addition to this study, two studies have quantified cytokines during regeneration—one in axolotl limbs (11) and the other in spiny mouse dorsal skin wounds (23). Godwin et al. (11)

used a mouse cytokine array to analyze regenerating salamander limbs and found that all but two cytokines detected reached peak amounts within 48 h of injury and that every cytokine returned to baseline by D15 after a blastema had formed. Brant et al. (23) used the same cytokine array to assess cytokines during the first 14 days of spiny mouse dorsal skin regeneration and observed a similar phenomenon with all detected cytokines resolving to baseline by D14. Despite study-specific differences in the ability to detect antigens and a lack of parallelism validation for the cytokine arrays used in these studies, their findings support that release of CCL3 and TNFα in tandem with a differential inflammatory response occurs prior to tissue regeneration. However, our comparative analyses also suggested that the magnitude of the increase in IL-6 and CXCL1 might serve as early indicators of a fibrotic repair trajectory. For example, the IL-6 response to injury, although present, was small and CXCL1 did not respond during both axolotl limb and spiny mouse skin regeneration.

Finally, our cellular analysis uncovered a surprisingly rapid adaptive immune response measured as an early influx of CD3+ T cells in regenerating compared to non-regenerating species. Importantly, our findings support that the arrival of T cells in spiny mice is concurrent with the arrival and proliferation of monocytes (16), which suggests there is a regenerative-competent T cell response that is different from a fibrotic T cell response. Contrary to hypotheses suggesting that a strong adaptive immune response reduces regenerative ability (91, 92), our findings suggest T cells may positively regulate regeneration in spiny mice and at the very least are not inhibitory. Similar to macrophages, T cells can differentiate into a number of functional subpopulations which differentially affect cells in the inflammatory microenvironment (93). Our analysis of the transcriptional response to injury between *M. musculus* and *A. cahirinus* suggests that fibrotic repair is associated with an accumulation of inactivated T_H cells, while during regeneration there is an accumulation of activated cytotoxic T and regulatory T (T_{REG}) cells. Studies have shown that loss of cytotoxic $CD8^+$ T cells inhibits skeletal muscle regeneration, accelerates bone fracture healing, and increases fibrosis in incisional wounds (94–100). Additionally, recent work showed that T_{REG} populations infiltrate injured muscle quickly after injury and are necessary to regulate the ratio of MHC-class II positive and negative macrophages present in the injured tissue. When the T_{REG} population was ablated subsequent regeneration was impaired (18). Moreover, spiny mice have a greater NADPH oxidase induced ROS response (16), which can be partially controlled by T_{REG} cells (101–103). Along these lines, T_{REG} are also necessary for zebrafish fin regeneration (17), supporting the hypothesis that a "regeneration-specific" T_{REG} is necessary for the maintenance and transition to tissue regeneration. Thus, these studies support an anti-fibrotic role for T cells and suggest the action of T_{REG} cells likely have a positive role during spiny mouse epimorphic regeneration.

Together, the data presented here support that tissue regeneration in *Acomys* occurs in cooperation with an adaptive immune response and that lymphocyte phenotype might play a key role in facilitating a regenerative or fibrotic response. Ongoing studies in our laboratory are aimed at characterizing the macrophage and T cell populations that are associated with the injured tissue during regeneration and fibrotic repair and should yield insight along these lines. These future datasets (and the present one) will create a framework to begin testing how the immune response functions during complex tissue regeneration in a mammalian model. We believe that modulating the immune response at the injury microenvironment will be an essential piece to inducing epimorphic regeneration in tissues that naturally heal by fibrotic repair.

DATA AVAILABILITY STATEMENT

The raw data supporting the conclusions of this article will be made available by the authors, without undue reservation.

ETHICS STATEMENT

The animal study, trapping and procedures were approved by the University of Kentucky Institutional Animal Care and Use Committee (IACUC) under protocol 2013-1119, Kenyan Wildlife Service (KWS), and the University of Nairobi Faculty of Veterinary Medicine Animal Care and Use Committee (FVM ACUC). Research in Kenya was approved by the Kenyan National Council for Science and Technology (NACOSTI). All wild species trapped were species of least concern.

AUTHOR CONTRIBUTIONS

Conceptualization and supervision: TG, SK, VE, and AS. Methodology: TG, JS, VE, and AS. Validation: TG and JS. Investigation: TG, JS, JK, CH, VE, and AS. Resources and funding acquisition: SK, VE, and AS. Writing—original draft: TG. Writing—review & editing: TG, JS, VE, and AS. Visualization: TG and AS. Project administration: TG, VE, and AS. All authors contributed to the article and approved the submitted version.

FUNDING

ACKNOWLEDGMENTS

continued access to their property in Kenya. We acknowledge David Higginbotham, Jim Monegue and rest of the swine unit for their help and enthusiasm with trapping the wild *Mus musculus*. This manuscript has been released as a pre-print at bioRxiv (104).

SUPPLEMENTARY MATERIAL

The Supplementary Material for this article can be found online at: https://www.frontiersin.org/articles/10.3389/fimmu.2020.01695/full#supplementary-material

REFERENCES

1. Seifert AW, Maden M. New insights into vertebrate skin regeneration. *Int Rev Cell Mol Biol.* (2014) 310:129–69. doi: 10.1016/B978-0-12-800180-6.00004-9
2. Martin P. Wound healing–aiming for perfect skin regeneration. *Science.* (1997) 276:75–81. doi: 10.1126/science.276.5309.75
3. Carlson BM. *Principles of Regenerative Biology.* Amsterdam: Elsevier/Academic Press; Mass: Burlington (2007).
4. Harty M, Neff AW, King MW, Mescher AL. Regeneration or scarring: an immunologic perspective. *Dev Dyn.* (2003) 226:268–79. doi: 10.1002/dvdy.10239
5. Seifert AW, Muneoka K. The blastema and epimorphic regeneration in mammals. *Dev Biol.* (2017) 433:190–9. doi: 10.1016/j.ydbio.2017.08.007
6. Eming SA, Wynn TA, Martin P. Inflammation and metabolism in tissue repair and regeneration. *Science.* (2017) 356:1026–30. doi: 10.1126/science.aam7928
7. Stoecklein VM, Osuka A, Lederer JA. Trauma equals danger–damage control by the immune system. *J Leukoc Biol.* (2012) 92:539–51. doi: 10.1189/jlb.0212072
8. Mescher AL. Macrophages and fibroblasts during inflammation and tissue repair in models of organ regeneration. *Regeneration.* (2017) 4:39–53. doi: 10.1002/reg2.77
9. Simkin J, Seifert AW. Concise review: translating regenerative biology into clinically relevant therapies: are we on the right path? *Stem Cells Transl Med.* (2018) 7:220–31. doi: 10.1002/sctm.17-0213
10. Godwin JW, Brockes JP. Regeneration, tissue injury and the immune response. *J Anat.* (2006) 209:423–32. doi: 10.1111/j.1469-7580.2006.00626.x
11. Godwin JW, Pinto AR, Rosenthal NA. Macrophages are required for adult salamander limb regeneration. *Proc Natl Acad Sci USA.* (2013) 110:9415–20. doi: 10.1073/pnas.1300290110
12. Godwin JW, Debuque R, Salimova E, Rosenthal NA. Heart regeneration in the salamander relies on macrophage-mediated control of fibroblast activation and the extracellular landscape. *NPJ Regen Med.* (2017) 2:22. doi: 10.1038/s41536-017-0027-y
13. Petrie TA, Strand NS, Yang CT, Rabinowitz JS, Moon RT. Macrophages modulate adult zebrafish tail fin regeneration. *Development.* (2014) 141:2581–91. doi: 10.1242/dev.098459
14. Aurora AB, Porrello ER, Tan W, Mahmoud AI, Hill JA, Bassel-Duby R, et al. Macrophages are required for neonatal heart regeneration. *J Clin Invest.* (2014) 124:1382–92. doi: 10.1172/JCI72181
15. Simkin J, Sammarco MC, Marrero L, Dawson LA, Yan M, Tucker C, et al. Macrophages are required to coordinate mouse digit tip regeneration. *Development.* (2017) 144:3907–16. doi: 10.1101/104356
16. Simkin J, Gawriluk TR, Gensel JC, Seifert AW. Macrophages are necessary for epimorphic regeneration in African spiny mice. *Elife.* (2017) 6:e24623. doi: 10.7554/eLife.24623
17. Hui SP, Sheng DZ, Sugimoto K, Gonzalez-Rajal A, Nakagawa S, Hesselson D, et al. Zebrafish regulatory T cells mediate organ-specific regenerative programs. *Dev Cell.* (2017) 43:659–72.e5. doi: 10.1016/j.devcel.2017.11.010
18. Panduro M, Benoist C, Mathis D. Treg cells limit IFN-gamma production to control macrophage accrual and phenotype during skeletal muscle regeneration. *Proc Natl Acad Sci USA.* (2018) 115:E2585–93. doi: 10.1073/pnas.1800618115
19. Love NR, Chen Y, Ishibashi S, Kritsiligkou P, Lea R, Koh Y, et al. Amputation-induced reactive oxygen species are required for successful *Xenopus* tadpole tail regeneration. *Nat Cell Biol.* (2013) 15:222–8. doi: 10.1038/ncb2659

20. Gauron C, Rampon C, Bouzaffour M, Ipendey E, Teillon J, Volovitch M, et al. Sustained production of ROS triggers compensatory proliferation and is required for regeneration to proceed. *Sci Rep.* (2013) 3:2084. doi: 10.1038/srep02084
21. Ferreira F, Luxardi G, Reid B, Zhao M. Early bioelectric activities mediate redox-modulated regeneration. *Development.* (2016) 143:4582–94. doi: 10.1242/dev.142034
22. Saunders NR, Noor NM, Dziegielewska KM, Wheaton BJ, Liddelow SA, Steer DL, et al. Age-dependent transcriptome and proteome following transection of neonatal spinal cord of *Monodelphis domestica* (South American grey short-tailed opossum). *PLoS ONE.* (2014) 9:e99080. doi: 10.1371/journal.pone.0099080
23. Brant JO, Yoon JH, Polvadore T, Barbazuk WB, Maden M. Cellular events during scar-free skin regeneration in the spiny mouse, Acomys. *Wound Repair Regen.* (2016) 24:75–88. doi: 10.1111/wrr.12385
24. He L, Marneros AG. Macrophages are essential for the early wound healing response and the formation of a fibrovascular scar. *Am J Pathol.* (2013) 182:2407–17. doi: 10.1016/j.ajpath.2013.02.032
25. Nosbaum A, Prevel N, Truong HA, Mehta P, Ettinger M, Scharschmidt TC, et al. Cutting edge: regulatory T cells facilitate cutaneous wound healing. *J Immunol.* (2016) 196:2010–4. doi: 10.4049/jimmunol.1502139
26. Mirza R, DiPietro LA, Koh TJ. Selective and specific macrophage ablation is detrimental to wound healing in mice. *Am J Pathol.* (2009) 175:2454–62. doi: 10.2353/ajpath.2009.090248
27. Goren I, Allmann N, Yogev N, Schurmann C, Linke A, Holdener M, et al. A transgenic mouse model of inducible macrophage depletion: effects of diphtheria toxin-driven lysozyme M-specific cell lineage ablation on wound inflammatory, angiogenic, contractive processes. *Am J Pathol.* (2009) 175:132–47. doi: 10.2353/ajpath.2009.081002
28. Lucas T, Waisman A, Ranjan R, Roes J, Krieg T, Muller W, et al. Differential roles of macrophages in diverse phases of skin repair. *J Immunol.* (2010) 184:3964–77. doi: 10.4049/jimmunol.0903356
29. Huo Y, Qiu WY, Pan Q, Yao YF, Xing K, Lou MF. Reactive oxygen species (ROS) are essential mediators in epidermal growth factor (EGF)-stimulated corneal epithelial cell proliferation, adhesion, migration, wound healing. *Exp Eye Res.* (2009) 89:876–86. doi: 10.1016/j.exer.2009.07.012
30. Hopkinson-Woolley J, Hughes D, Gordon S, Martin P. Macrophage recruitment during limb development and wound healing in the embryonic and foetal mouse. *J Cell Sci.* (1994) 107(Pt 5):1159–67.
31. Whitby DJ, Ferguson MW. Immunohistochemical localization of growth factors in fetal wound healing. *Dev Biol.* (1991) 147:207–15. doi: 10.1016/S0012-1606(05)80018-1
32. Martin P, Dickson MC, Millan FA, Akhurst RJ. Rapid induction and clearance of TGF beta 1 is an early response to wounding in the mouse embryo. *Dev Genet.* (1993) 14:225–38. doi: 10.1002/dvg.1020140309
33. Mescher AL, Neff AW, King MW. Changes in the inflammatory response to injury and its resolution during the loss of regenerative capacity in developing *Xenopus* limbs. *PLoS ONE.* (2013) 8:e80477. doi: 10.1371/journal.pone.0080477
34. Robert J, Ohta Y. Comparative and developmental study of the immune system in *Xenopus*. *Dev Dyn.* (2009) 238:1249–70. doi: 10.1002/dvdy.21891
35. Bertolotti E, Malagoli D, Franchini A. Skin wound healing in different aged *Xenopus laevis*. *J Morphol.* (2013) 274:956–64. doi: 10.1002/jmor.20155
36. Mak K, Manji A, Gallant-Behm C, Wiebe C, Hart DA, Larjava H, et al. Scarless healing of oral mucosa is characterized by faster resolution of inflammation and control of myofibroblast action compared to skin wounds in the red Duroc pig model. *J Dermatol Sci.* (2009) 56:168–80. doi: 10.1016/j.jdermsci.2009.09.005

37. Szpaderska AM, Zuckerman JD, DiPietro LA. Differential injury responses in oral mucosal and cutaneous wounds. *J Dent Res.* (2003) 82:621–6. doi: 10.1177/154405910308200810

38. Chen L, Arbieva ZH, Guo S, Marucha PT, Mustoe TA, DiPietro LA. Positional differences in the wound transcriptome of skin and oral mucosa. *BMC Genomics.* (2010) 11:471. doi: 10.1186/1471-2164-11-471

39. Fini ME, Sicard RE. Limb regeneration of the adult newt (*Notophthalmus viridescens*) in the absence of the spleen. *Wilehm Roux Arch Dev Biol.* (1980) 189:77–9. doi: 10.1007/BF00848570

40. Schotte OE, Sicard RE. Cyclophosphamide-induced leukopenia and suppression of limb regeneration in the adult newt, *Notophthalmus viridescens*. *J Exp Zool.* (1982) 222:199–202. doi: 10.1002/jez.1402220212

41. Gawriluk TR, Simkin J, Thompson KL, Biswas SK, Clare-Salzler Z, Kimani JM, et al. Comparative analysis of ear-hole closure identifies epimorphic regeneration as a discrete trait in mammals. *Nat Commun.* (2016) 7:11164. doi: 10.1038/ncomms11164

42. Matias DS, Martins AR, Casanellas I, Ova AB, Araújo IM, Power D, et al. Ear wound regeneration in the African spiny mouse *acomys cahirinus*. *Regeneration*. (2015) 3:52– 61. doi: 10.1002/reg2.50

43. Seifert AW, Kiama SG, Seifert MG, Goheen JR, Palmer TM, Maden M. Skin shedding and tissue regeneration in African spiny mice (*Acomys*). *Nature*. (2012) 489:561–5. doi: 10.1038/nature11499

44. Haughton CL, Gawriluk TR, Seifert AW. The biology and husbandry of the african spiny mouse (*Acomys cahirinus*) and the research uses of a laboratory colony. *J Am Assoc Lab Anim Sci.* (2016) 55:9–17.

45. Plikaytis BD, Holder PF, Pais LB, Maslanka SE, Gheesling LL, Carlone GM. Determination of parallelism and nonparallelism in bioassay dilution curves. *J Clin Microbiol.* (1994) 32:2441–7. doi: 10.1128/JCM.32.10.2441-2447.1994

46. Tu J, Bennett P. Parallelism experiments to evaluate matrix effects, selectivity and sensitivity in ligand-binding assay method development: pros and cons. *Bioanalysis.* (2017) 9:1107–22. doi: 10.4155/bio-2017-0084

47. Mamrot J, Legaie R, Ellery SJ, Wilson T, Seemann T, Powell DR, et al. *De novo* transcriptome assembly for the spiny mouse (*Acomys cahirinus*). *Sci Rep.* (2017) 7:8996. doi: 10.1038/s41598-017-09334-7

48. Katoh K, Misawa K, Kuma K, Miyata T. MAFFT: a novel method for rapid multiple sequence alignment based on fast fourier transform. *Nucleic Acids Res.* (2002) 30:3059–66. doi: 10.1093/nar/gkf436

49. Katoh K, Rozewicki J, Yamada KD. MAFFT online service: multiple sequence alignment, interactive sequence choice and visualization. *Brief Bioinform.* (2017) 20:1160–6. doi: 10.1093/bib/bbx108

50. Whitcomb BW, Schisterman EF. Assays with lower detection limits: implications for epidemiological investigations. *Paediatr Perinat Epidemiol.* (2008) 22:597–602. doi: 10.1111/j.1365-3016.2008.00969.x

51. Rueden CT, Schindelin J, Hiner MC, DeZonia BE, Walter AE, Arena ET, et al. ImageJ2: imageJ for the next generation of scientific image data. *BMC Bioinformatics.* (2017) 18:529. doi: 10.1186/s12859-017-1934-z

52. Lesher A, Li B, Whitt P, Newton N, Devalapalli AP, Shieh K, et al. Increased IL-4 production and attenuated proliferative and pro-inflammatory responses of splenocytes from wild-caught rats (*Rattus norvegicus*). *Immunol Cell Biol.* (2006) 84:374–82. doi: 10.1111/j.1440-1711.2006.01440.x

53. Titus RG, Sherry B, Cerami A. The involvement of TNF, IL-1 and IL-6 in the immune response to protozoan parasites. *Immunol Today.* (1991) 12:A13–6. doi: 10.1016/S0167-5699(05)80005-2

54. Viney M, Riley EM. The immunology of wild rodents: current status and future prospects. *Front Immunol.* (2017) 8:1481. doi: 10.3389/fimmu.2017.01481

55. Julier Z, Park AJ, Briquez PS, Martino MM. Promoting tissue regeneration by modulating the immune system. *Acta Biomater.* (2017) 53:13–28. doi: 10.1016/j.actbio.2017.01.056

56. Trinchieri G, Pflanz S, Kastelein RA. The IL-12 family of heterodimeric cytokines: new players in the regulation of T cell responses. *Immunity*. (2003) 19:641–4. doi: 10.1016/S1074-7613(03)00296-6

57. Weaver CT, Hatton RD, Mangan PR, Harrington LE. IL-17 family cytokines and the expanding diversity of effector T cell lineages. *Annu Rev Immunol.* (2007) 25:821–52. doi: 10.1146/annurev.immunol.25.022106.141557

58. Heinrich PC, Behrmann I, Muller-Newen G, Schaper F, Graeve L. Interleukin-6-type cytokine signalling through the gp130/Jak/STAT pathway. *Biochem J.* (1998) 334 (Pt 2):297–314. doi: 10.1042/bj3340297

59. Hunter CA, Jones SA. Corrigendum: IL-6 as a keystone cytokine in health and disease. *Nat Immunol.* (2017) 18:1271. doi: 10.1038/ni1117-1271b

60. Tanaka T, Narazaki M, Kishimoto T. IL-6 in inflammation, immunity, and disease. *Cold Spring Harb Perspect Biol.* (2014) 6:a016295. doi: 10.1101/cshperspect.a016295

61. Kroeze KL, Boink MA, Sampat-Sardjoepersad SC, Waaijman T, Scheper RJ, Gibbs S. Autocrine regulation of re-epithelialization after wounding by chemokine receptors CCR1, CCR10, CXCR1, CXCR2, and CXCR3. *J Invest Dermatol.* (2012) 132:216–25. doi: 10.1038/jid.2011.245

62. Lin ZQ, Kondo T, Ishida Y, Takayasu T, Mukaida N. Essential involvement of IL-6 in the skin wound-healing process as evidenced by delayed wound healing in IL-6-deficient mice. *J Leukoc Biol.* (2003) 73:713–21. doi: 10.1189/jlb.0802397

63. Gallucci RM, Simeonova PP, Matheson JM, Kommineni C, Guriel JL, Sugawara T, et al. Impaired cutaneous wound healing in interleukin-6-deficient and immunosuppressed mice. *FASEB J.* (2000) 14:2525–31. doi: 10.1096/fj.00-0073com

64. Devalaraja RM, Nanney LB, Du J, Qian Q, Yu Y, Devalaraja MN, et al. Delayed wound healing in CXCR2 knockout mice. *J Invest Dermatol.* (2000) 115:234–44. doi: 10.1046/j.1523-1747.2000.00034.x

65. McFarland-Mancini MM, Funk HM, Paluch AM, Zhou M, Giridhar PV, Mercer CA, et al. Differences in wound healing in mice with deficiency of IL-6 versus IL-6 receptor. *J Immunol.* (2010) 184:7219–28. doi: 10.4049/jimmunol.0901929

66. Wu KK. Cyclooxygenase 2 induction: molecular mechanism and pathophysiologic roles. *J Lab Clin Med.* (1996) 128:242–5. doi: 10.1016/S0022-2143(96)90023-2

67. Penning TD, Talley JJ, Bertenshaw SR, Carter JS, Collins PW, Docter S, et al. Synthesis and biological evaluation of the 1,5-diarylpyrazole class of cyclooxygenase-2 inhibitors: identification of 4-[5-(4-methylphenyl)-3-(trifluoromethyl)-1H-pyrazol-1-yl]benze nesulfonamide (SC-58635, celecoxib). *J Med Chem.* (1997) 40:1347–65.

68. Beura LK, Hamilton SE, Bi K, Schenkel JM, Odumade OA, Casey KA, et al. Normalizing the environment recapitulates adult human immune traits in laboratory mice. *Nature*. (2016) 532:512–6. doi: 10.1038/nature17655

69. Abolins S, King EC, Lazarou L, Weldon L, Hughes L, Drescher P, et al. The comparative immunology of wild and laboratory mice, *Musculus domesticus*. *Nat Commun.* (2017) 8:14811. doi: 10.1038/ncomms14811

70. Martin P, Leibovich SJ. Inflammatory cells during wound repair: the good, the bad and the ugly. *Trends Cell Biol.* (2005) 15:599–607. doi: 10.1016/j.tcb.2005.09.002

71. Hildebrand F, Hubbard WJ, Choudhry MA, Frink M, Pape HC, Kunkel SL, et al. Kupffer cells and their mediators: the culprits in producing distant organ damage after trauma-hemorrhage. *Am J Pathol.* (2006) 169:784–94. doi: 10.2353/ajpath.2006.060010

72. Deshmane SL, Kremlev S, Amini S, Sawaya BE. Monocyte chemoattractant protein-1 (MCP-1): an overview. *J Interferon Cytokine Res.* (2009) 29:313–26. doi: 10.1089/jir.2008.0027

73. Low QE, Drugea IA, Duffner LA, Quinn DG, Cook DN, Rollins BJ, et al. Wound healing in MIP-1alpha(-/-) and MCP-1(-/-) mice. *Am J Pathol.* (2001) 159:457–63. doi: 10.1016/S0002-9440(10)61717-8

74. Ziraldo C, Vodovotz Y, Namas RA, Almahmoud K, Tapias V, Mi Q, et al. Central role for MCP-1/CCL2 in injury-induced inflammation revealed by *in vitro*, *in silico*, clinical studies. *PLoS ONE.* (2013) 8:e79804. doi: 10.1371/journal.pone.0079804

75. Sierra-Filardi E, Nieto C, Dominguez-Soto A, Barroso R, Sanchez-Mateos P, Puig-Kroger A, et al. CCL2 shapes macrophage polarization by GM-CSF and M-CSF: identification of CCL2/CCR2-dependent gene expression profile. *J Immunol.* (2014) 192:3858–67. doi: 10.4049/jimmunol.1302821

76. Lu B, Rutledge BJ, Gu L, Fiorillo J, Lukacs NW, Kunkel SL, et al. Abnormalities in monocyte recruitment and cytokine expression in monocyte chemoattractant protein 1-deficient mice. *J Exp Med.* (1998) 187:601–8. doi: 10.1084/jem.187.4.601

77. Wynn TA, Vannella KM. Macrophages in tissue repair, regeneration, and fibrosis. *Immunity.* (2016) 44:450–62. doi: 10.1016/j.immuni.2016.02.015

78. Leibovich S, Ross R. The role of the macrophage in wound repair. a study with hydrocortisone and antimacrophage serum. *A J Pathol.* (1975) 78:71.

79. Simkin J, Sammarco MC, Marrero L, Dawson LA, Yan M, Tucker C, et al. Macrophages are required to coordinate mouse digit tip regeneration. *Development.* (2017) 144:3907–16. doi: 10.1242/dev.150086

80. Shook B, Xiao E, Kumamoto Y, Iwasaki A, Horsley V. CD301b+ macrophages are essential for effective skin wound healing. *J Invest Dermatol.* (2016) 136:1885–91. doi: 10.1016/j.jid.2016.05.107

81. Gschwandtner M, Derler R, Midwood KS. More than just attractive: how CCL2 influences myeloid cell behavior beyond chemotaxis. *Front Immunol.* (2019) 10:2759. doi: 10.3389/fimmu.2019.02759

82. Pellegrino MJ, Habecker BA. STAT3 integrates cytokine and neurotrophin signals to promote sympathetic axon regeneration. *Mol Cell Neurosci.* (2013) 56:272–82. doi: 10.1016/j.mcn.2013.06.005

83. Qin S, Zou Y, Zhang CL. Cross-talk between KLF4 and STAT3 regulates axon regeneration. *Nat Commun.* (2013) 4:2633. doi: 10.1038/ncomms3633

84. Zhu H, Xiao F, Wang G, Wei X, Jiang L, Chen Y, et al. STAT3 regulates self-renewal of adult muscle satellite cells during injury-induced muscle regeneration. *Cell Rep.* (2016) 16:2102–15. doi: 10.1016/j.celrep.2016.07.041

85. Bard JD, Gelebart P, Amin HM, Young LC, Ma Y, Lai R. Signal transducer and activator of transcription 3 is a transcriptional factor regulating the gene expression of SALL4. *FASEB J.* (2009) 23:1405–14. doi: 10.1096/fj.08-117721

86. Grow M, Neff AW, Mescher AL, King MW. Global analysis of gene expression in *Xenopus hindlimbs* during stage-dependent complete and incomplete regeneration. *Dev Dyn.* (2006) 235:2667–85. doi: 10.1002/dvdy.20897

87. Neff AW, King MW, Mescher AL. Dedifferentiation and the role of sall4 in reprogramming and patterning during amphibian limb regeneration. *Dev Dyn.* (2011) 240:979–89. doi: 10.1002/dvdy.22554

88. Fairweather M, Heit YI, Buie J, Rosenberg LM, Briggs A, Orgill DP, et al. Celecoxib inhibits early cutaneous wound healing. *J Surg Res.* (2015) 194:717–24. doi: 10.1016/j.jss.2014.12.026

89. Romana-Souza B, Santos JS, Bandeira LG, Monte-Alto-Costa A. Selective inhibition of COX-2 improves cutaneous wound healing of pressure ulcers in mice through reduction of iNOS expression. *Life Sci.* (2016) 153:82–92. doi: 10.1016/j.lfs.2016.04.017

90. Wilgus TA, Vodovotz Y, Vittadini E, Clubbs EA, Oberyszyn TM. Reduction of scar formation in full-thickness wounds with topical celecoxib treatment. *Wound Repair Regen.* (2003) 11:25–34. doi: 10.1046/j.1524-475X.2003.11106.x

91. Godwin JW, Rosenthal N. Scar-free wound healing and regeneration in amphibians: immunological influences on regenerative success. *Differentiation.* (2014) 87:66–75. doi: 10.1016/j.diff.2014.02.002

92. Mescher AL, Neff AW, King MW. Inflammation and immunity in organ regeneration. *Dev Comp Immunol.* (2017) 66:98–110. doi: 10.1016/j.dci.2016.02.015

93. Hirahara K, Nakayama T. CD4+ T-cell subsets in inflammatory diseases: beyond the Th1/Th2 paradigm. *Int Immunol.* (2016) 28:163–71. doi: 10.1093/intimm/dxw006

94. Barbul A, Breslin RJ, Woodyard JP, Wasserkrug HL, Efron G. The effect of *in vivo* T helper and T suppressor lymphocyte depletion on wound healing. *Ann Surg.* (1989) 209:479–83. doi: 10.1097/00000658-198904000-0 0015

95. Barbul A, Shawe T, Rotter SM, Efron JE, Wasserkrug HL, Badawy SB. Wound healing in nude mice: a study on the regulatory role of lymphocytes in fibroplasia. *Surgery.* (1989) 105:764–9.

96. Barbul A, Sisto D, Rettura G, Levenson SM, Seifter E, Efron G. Thymic inhibition of wound healing: abrogation by adult thymectomy. *J Surg Res.* (1982) 32:338–42. doi: 10.1016/0022-4804(82)90110-X

97. Fishel R, Barbul A, Wasserkrug HL, Penberthy LT, Rettura G, Efron G. Cyclosporine A impairs wound healing in rats. *J Surg Res.* (1983) 34:572–5. doi: 10.1016/0022-4804(83)90112-9

98. Peterson JM, Barbul A, Breslin RJ, Wasserkrug HL, Efron G. Significance of T-lymphocytes in wound healing. *Surgery.* (1987) 102:300–5.

99. Zhang J, Xiao Z, Qu C, Cui W, Wang X, Du J. CD8 T cells are involved in skeletal muscle regeneration through facilitating MCP-1 secretion and Gr1(high) macrophage infiltration. *J Immunol.* (2014) 193:5149–60. doi: 10.4049/jimmunol.1303486

100. Reinke S, Geissler S, Taylor WR, Schmidt-Bleek K, Juelke K, Schwachmeyer V, et al. Terminally differentiated CD8(+) T cells negatively affect bone regeneration in humans. *Sci Transl Med.* (2013) 5:177ra36. doi: 10.1126/scitranslmed.3004754

101. Kwon J, Devadas S, Williams MS. T cell receptor-stimulated generation of hydrogen peroxide inhibits MEK-ERK activation and lck serine phosphorylation. *Free Radic Biol Med.* (2003) 35:406–17. doi: 10.1016/S0891-5849(03)00318-6

102. Kim HR, Lee A, Choi EJ, Hong MP, Kie JH, Lim W, et al. Reactive oxygen species prevent imiquimod-induced psoriatic dermatitis through enhancing regulatory T cell function. *PLoS ONE.* (2014) 9:e91146. doi: 10.1371/journal.pone.0091146

103. Kraaij MD, Savage ND, van der Kooij SW, Koekkoek K, Wang J, van den Berg JM, et al. Induction of regulatory T cells by macrophages is dependent on production of reactive oxygen species. *Proc Natl Acad Sci USA.* (2010) 107:17686–91. doi: 10.1073/pnas.1012016107

104. Gawriluk TR, Simkin J, Hacker CK, Kimani JM, Kiama SG, Ezenwa VO, et al. Mammalian musculoskeletal regeneration is associated with reduced inflammatory cytokines and an influx of T cells. *bioRxiv.* (2019) 723783. doi: 10.1101/723783